Experimental and Theoretical Investigations of Infrared Multiple Photon Dissociation Spectra of Aspartic Acid Complexes with Zn^{2+} and Cd^{2+}

Georgia C. Boles,[†] Randy L. Hightower,[†] Rebecca A. Coates,[†,%] Christopher P. McNary,[†] Giel Berden,[‡] Jos Oomens,[‡,#] and P. B. Armentrout[*,†]*

[†]Department of Chemistry, University of Utah, 315 S. 1400 E. Rm. 2020, Salt Lake City, Utah 84112, United States

[‡]Radboud University, Institute for Molecules and Materials, FELIX Laboratory, Toernooiveld 7c, NL-6525 ED Nijmegen, The Netherlands

[#]van't Hoff Institute for Molecular Sciences, University of Amsterdam, Amsterdam, The Netherlands

* Corresponding author, e-mail: armentrout@chem.utah.edu

[%] Present address: Department of Chemistry, Central Washington University, 400 E. University Way, Ellensburg, WA 98926

Abstract: Complexes of aspartic acid (Asp) cationized with Zn^{2+}: $Zn(Asp\text{-}H)^+$, $Zn(Asp\text{-}H)^+(ACN)$ where ACN = acetonitrile, and $Zn(Asp\text{-}H)^+(Asp)$, as well as with Cd^{2+}, $CdCl^+(Asp)$, were examined by infrared multiple photon dissociation (IRMPD) action spectroscopy using light generated from a free electron laser. A series of low-energy conformers for each complex was found using quantum chemical calculations in order to identify the structures formed experimentally. The main binding motif observed for the heavy metal complex, $CdCl^+(Asp)[N,CO,CO_s]$, is a charge solvated, tridentate structure where the metal center binds to the backbone amino group and carbonyl oxygens of the backbone and side-chain carboxylic acids. Likewise, the deprotonated $Zn(Asp\text{-}H)^+(ACN)$ and $Zn(Asp\text{-}H)^+(Asp)$ complexes show comparable $[N,CO^-,CO_s](ACN)$ and $[N,CO^-,CO_s][N,CO,CO_s]$ coordination, respectively. Interestingly, there was only minor spectral evidence for the analogous $Zn(Asp\text{-}H)^+[N,CO^-,CO_s]$ binding motif, even though this species is predicted to be the lowest energy conformer. Instead,

rearrangement and partial dissociation of the amino acid is observed, as spectral features most consistent with the experimental spectrum are exhibited by a four-coordinate $Zn(Asp\text{-}NH_4)^+$ $[CO_2^-,CO_s](NH_3)$ complex. Analysis of the mechanistic pathway leading from the predicted lowest energy conformer to the isobaric deaminated complex is explored theoretically. Further, comparison of the current work to that of Zn^{2+} and Cd^{2+} complexes of asparagine (Asn) allow additional conclusions regarding populated conformers and effects of carboxamide versus carboxylic acid binding to be drawn.

Introduction

The utilization of infrared multiple photon dissociation (IRMPD) spectroscopy to study cationized amino acid complexes has been well documented.[1-15] Our group has previously studied the complexes of histidine (His),[9] cysteine (Cys) and cysteine methyl ester (Cys-OMe),[11] glutamine (Gln),[12] serine (Ser),[13] asparagine (Asn),[14] and glutamic acid (Glu)[15] cationized with Zn^{2+} and Cd^{2+}, as these two metals play an important role in binding to proteins under biological conditions, particularly in zinc finger domains.[16,17] Zn^{2+} has been shown to bind preferentially to Cys and His residues under various experimental conditions,[18] although it is not obvious why those amino acids are preferred. The replacement of Zn^{2+} centers with Cd^{2+} and other cations has been reported; however, the nature of the metal dependence of these systems is not yet completely understood.[19,20] Previous IRMPD studies of the complexes mentioned above have elucidated important structural information regarding the metal dependence of the systems of interest.[9,11-15] In the current work, we continue this evaluation by examining the structural and energetic characteristics of aspartic acid (Asp) binding to these Zn^{2+} and Cd^{2+} metals. Furthermore, the study of Asp has additional biological relevance regarding its role in the deamidation of Asn residues, where deamidation followed by hydrolysis (under physiological conditions) has been shown to yield a combination of Asp and iso-Asp.[21] Deamidation of Asn residues (and subsequent production of excess iso-Asp residues) is commonly associated with protein degradation and has been linked to the onset and progression of Parkinson's and Alzheimer's diseases.[22]

In order to definitively determine conformations of the complexes formed experimentally, IRMPD action spectra for each complex were measured. Experimental spectra were then compared to spectra calculated for a series of low-energy conformers with optimized structures and vibrational frequencies determined at the B3LYP/6-311+G(d,p) or B3LYP/def2-TZVP level of theory. Comparison of the calculated and experimental spectra of all systems allow for clear identification of the populated conformations. Analysis of these complexes allows for a more complete understanding of the metal dependence of these and other systems, where we are particularly interested in the fundamental nature of metal-amino acid interactions in important physiological processes.

Experimental and Computational Section

Mass Spectrometry and Photodissociation. Experiments were performed at the free electron lasers for infrared experiments (FELIX) facility at Radboud University in the Netherlands.[23] A 4.7 T Fourier transform ion cyclotron resonance (FT-ICR) mass spectrometer, described elsewhere, was used to measure the IRMPD spectra.[24-26] Ions were generated using an electrospray ionization (ESI) source and then accumulated in a hexapole trap for about 4 s before being pulse extracted through a quadrupole bender and injected into the ICR cell via a radiofrequency (rf) octopole ion guide. Electrostatic switching of the dc bias of the octopole was used to avoid collisional heating of the ions.[25] Once trapped in the ICR cell, the ions of interest (assumed to be roughly at room temperature) were mass selected using a stored waveform inverse Fourier transform (SWIFT) excitation pulse.[27,28] These ions were irradiated with FELIX for 2 – 3 s at a 10 Hz macropulse repetition rate (energy up to 45 mJ per pulse and a bandwidth of 0.5% of the central frequency). The IRMPD spectra were generated by plotting the photofragmentation yield, $Y = \Sigma I_F / (\Sigma I_P + \Sigma I_F)$, where I_P and I_F are the integrated intensities of the precursor and fragment ion mass peaks (where the sum includes all isotopes), respectively, as a function of the frequency of IR radiation. The yield was linearly corrected for frequency dependent variation in the laser pulse energy, which can result in yields slight greater than one, as discussed further below.

The application of a linear laser power correction is well described in the literature[29] and is appropriate because the power dependence is basically linear until saturation begins because of the incoherent rather than coherent nature of the multiple photon excitation process. In one case, a depletion spectrum (defined as $-\ln(\Sigma I_P / \Sigma I_P^\circ)$, where I_P° is the integrated intensity of the precursor ion mass peak without irradiation) is shown in addition to ion yield. Here too, the depletion is corrected for frequency dependent variations in the laser pulse energy.

Metalated Asp complexes were prepared from solutions of 1.0 mM Asp and 1.0 mM $Zn(NO_3)_2$, $ZnCl_2$, or $CdCl_2$ in 60:40 MeOH/H_2O solvent using a Micromass Z-Spray ESI source. Flow rates of 6 μL/min were used, and the electrospray needle was held at a voltage of 3.0 kV. In the case of Zn^{2+}, the ESI source generated $Zn(Asp\text{-}H)^+(ACN)$ and $Zn(Asp\text{-}H)^+(Asp)$ complexes, in which the aspartic acid is deprotonated and an acetonitrile (ACN, CH_3CN) or additional aspartic acid ligand is bound. (The ACN was present adventitiously from previous experiments, although additional ACN was added to the solution in an effort to increase ion intensity). A 30 W continuous wave CO_2 laser was used to irradiate either of these complexes for 0.3 s, which removes the ACN or Asp ligand, yielding $Zn(Asp\text{-}H)^+$, and led to dissociation by loss of $C_4H_2O_3$ yielding a *m/z* 139 product ion in the case of $Zn(Asp\text{-}H)^+(ACN)$. These resulting ions were mass isolated and allowed to cool radiatively for 0.4 s.[30] Electrospray of the Cd^{2+} solution generated $CdCl^+(Asp)$, which did not dissociate upon CO_2 laser irradiation.

Computational Details. In order to determine low-lying conformers of the cationized Asp complexes, previously optimized $Zn(Asn\text{-}H)^+$ and $CdCl^+(Asn)$ complexes[14] were used as initial starting geometries, where the Asn carboxamide side-chain was replaced with an Asp carboxylic acid side-chain. For all complexes, the Gaussian 09 suite of programs was used.[31] Initial optimizations of the metalated complexes were then done at the B3LYP/6-31G(d) level of theory using the "loose" keyword to utilize a large step size of 0.01 au and an rms force constant of 0.0017 to facilitate convergence. Unique structures were then further optimized at the B3LYP/6-311+G(d,p) level of theory for Zn^{2+} complexes and at the B3LYP/def2-TZVP level, where def2-TZVP is a size-consistent basis set for all atoms and includes triple-ζ + polarization functions with

a small core (28 electron) effective core potential (ECP) on Cd.[32,33] The def2-TZVP basis set and corresponding ECP were obtained from the EMSL basis set exchange.[34] These combinations of level of theory, basis set, and SDD ECP have previously proven to provide accurate structural information with complexes of similar size and composition.[11-15] Geometry optimizations of metalated structures were also conducted including corrections for empirical dispersion at the B3LYP-GD3BJ level.[35,36] As will be discussed further in later sections, dissociation pathways were explored from these species such that we could predict conformers that may be adopted after irradiation with the CO_2 laser.

Vibrational frequencies were scaled by 0.975 for comparison to the IRMPD spectra, where this scaling factor has been show to account for known inaccuracies in the calculated frequencies, and therefore gives good agreement with well-resolved peaks in other IRMPD spectra.[9,11-15] The calculated frequencies were broadened using a 30 cm^{-1} full-width at half maximum Gaussian line shape when used for comparison to the experimentally determined spectra. This broadening accounts for the finite laser bandwidth, unresolved rotational structure of the ions (which are near room temperature), anharmonicity of the vibrational mode, and broadening as a result of the multiple photon absorption process.[37]

Relative energies were determined from B3LYP geometries using single point energies calculated at the B3LYP, B3P86, and MP2(full) levels using 6-311+G(2d,2p) (Zn^{2+} complexes) and def2-TZVPP (Cd^{2+} complexes) basis sets. Relative B3LYP-GD3BJ single point energies using these larger basis sets and the B3LYP-GD3BJ geometries were also computed. Zero point energy (ZPE) corrections were applied to single point energies in order to provide 0 K relative enthalpies. Thermal corrections to obtain 298 K Gibbs free energies were calculated from 0 K relative enthalpies by using the rigid rotor/harmonic oscillator approximation with the calculated rotational constants and vibrational frequencies. Vibrational frequencies were scaled by 0.989 when used for zero point energy (ZPE) and thermal corrections.[38]

Results and Discussion

IRMPD Action Spectroscopy. IRMPD action spectra were measured for zinc and cadmium complexes, where the main product fragments in each case were used to determine the yield spectrum. Here, we report the spectral region scanned from 5.5 to 10 μm (1000 – 1800 cm^{-1}). Linear corrections of the laser power were applied, which result in higher relative intensities of the high frequency bands and minor changes in the low frequency region. Notably, the intensity in the 1600 – 1700 cm^{-1} region was approximately doubled because of the linear power correction such that yields slightly greater than one were calculated for two systems.

The IRMPD spectrum of $Zn(Asp\text{-}H)^+(ACN)$ resulted in the fragmentation pattern shown in reactions 1 – 3 where the number in brackets indicates the mass to charge ratio (*m/z*) of the ion. Because ^{64}Zn is the most abundant isotope (49.17% natural abundance), the complex of this isotope is designated here as the precursor ion. Channels corresponding to ^{66}Zn and ^{68}Zn (27.73 and 18.45% natural abundance, respectively)[39] were also monitored and included in yield calculations for all Zn complexes shown in Figure 1, except for the dissociation products of $Zn(Asp\text{-}H)^+(ACN)$: $Zn(Asp\text{-}H)^+$ along with $ZnOH^+(NH_3)(ACN)$ discussed below. For these two species, ^{64}Zn and ^{66}Zn complexes were included in the dominant *m/z* 139 dissociation channel, but only ^{64}Zn complexes were observed with sufficient intensity for the additional dissociation channels of reactions 1 and 3.

$$Zn(Asp\text{-}H)^+(ACN)\ [237] + n\ h\nu \rightarrow Zn(Asp\text{-}H)^+\ [196] + ACN \quad (1)$$

$$\rightarrow ZnOH^+(NH_3)(ACN)\ [139] + (C_4H_2O_3) \quad (2)$$

$$Zn(Asp\text{-}H)^+\ [196] + n\ h\nu \rightarrow Zn(C_3H_6O_2N)^+\ [152] + CO_2 \quad (3)$$

IRMPD of $Zn(Asp\text{-}H)^+(ACN)$ resulted in bifurcating pathways, leading to reactions 1 and 2. The main dissociation pathway (with intensities dominating the *m/z* 196 channel across the entire spectral range analyzed) leads to $ZnOH^+(NH_3)(ACN)$ (where this identification is confirmed spectroscopically, see below), loss of $C_4H_2O_3$ in reaction 2. As shown in reaction 1, $Zn(Asp\text{-}H)^+(ACN)$ also undergoes ACN dissociation, substantially different dissociation behavior than observed with $Zn(Glu\text{-}H)^+(ACN)$, where no ACN dissociation was observed.[15] The $Zn(Asp\text{-}H)^+$ product sequentially dissociated by loss of CO_2, as shown in reaction 3. For the similar

$Zn(Asp\text{-}H)^+(Asp)$ system, the reaction analogous to process 1 (loss of intact Asp) was observed, followed by reaction 3. Representative mass spectra are given in Supporting Information Figure S1.

As described above, CO_2 laser irradiation can be used to generate the $Zn(Asp\text{-}H)^+$ complex in the FTICR cell from either the ACN or Asp complex or to generate $ZnOH^+(NH_3)(ACN)$ from $Zn(Asp\text{-}H)^+(ACN)$. For spectral comparisons in following sections, the $Zn(Asp\text{-}H)^+$ experimental spectrum measured from the $Zn(Asp\text{-}H)^+(Asp)$ precursor is used, Figure 1. The IRMPD spectrum resulting from the $Zn(Asp\text{-}H)^+(ACN)$ complex is given in Supporting Information Figure S2, where all main spectral features are reproduced. Subsequent IRMPD of $Zn(Asp\text{-}H)^+$ resulted in the fragmentation pattern corresponding to reactions 3 and 4.

$$Zn(C_3H_6O_2N)^+ [152] + n\ h\nu \rightarrow Zn(C_3H_3O_2)^+ [135] + NH_3 \qquad (4)$$

The major product appears at *m/z* 152 and results from the loss of CO_2, analogous to processes observed in previous studies of the similar Asn and Gln systems.[12,14] As shown by reaction 4, secondary ammonia loss occurs from *m/z* 152, where loss of CO_2, followed by NH_3 loss were observed in the $Zn(Asn\text{-}H)^+$ system as well.[12] Unlike the $Zn(Asn\text{-}H)^+$ system, however, the secondary NH_3 loss from $Zn(Asp\text{-}H)^+$ exhibited a much higher intensity and was therefore included in the yield measurement of the spectrum. A representative mass spectrum is given in Supporting Information Figure S3. IRMPD of the $ZnOH^+(NH_3)(ACN)$ species yielded losses of NH_3 and H_2O, with the IRMPD spectrum shown in Supporting Information Figure S4. A thorough discussion of the observed dissociation pathways is included in following sections.

As shown in Figure 1, the main spectral features of the $Zn(Asp\text{-}H)^+(ACN)$ and $Zn(Asp\text{-}H)^+(Asp)$ IRMPD spectra are distinctly different from those observed in the $Zn(Asp\text{-}H)^+$ spectrum. In particular, two carbonyl stretches (1748 and 1656 cm^{-1}) are observed in the $Zn(Asp\text{-}H)^+(ACN)$ spectrum, whereas only one broad band is observed in the $Zn(Asp\text{-}H)^+$ spectrum. Similarly, this $Zn(Asp\text{-}H)^+$ band is significantly red shifted with respect to the broad band in the high frequency CO stretching region of the $Zn(Asp\text{-}H)^+(Asp)$ spectrum. As detailed

below, identification of the conformers populated for $Zn(Asp\text{-}H)^+(ACN)$ and $Zn(Asp\text{-}H)^+(Asp)$ is valuable, and permits a more rigorous evaluation of the $Zn(Asp\text{-}H)^+$ complex structure.

The IRMPD of $CdCl^+(Asp)$ resulted in two major fragments, which appeared at *m/z* 236 and *m/z* 192, as shown in reactions 5 and 6. Masses are chosen to correspond to the most abundant isotopes of Cd and Cl, ^{114}Cd (28.75 %) and ^{35}Cl (75.5 %),[39] such that *m/z* 282 is designated as the precursor ion. The $CdCl^+(Asp)$ complexes associated with *m/z* values corresponding to ^{113}Cd (12.23 %), ^{112}Cd (24.11 %), ^{111}Cd (12.80 %), ^{110}Cd (12.47 %), and ^{37}Cl (24.5 %) were also monitored and included in yield calculations shown in Figure 1. Representative mass spectra are given in Supporting Information Figure S5.

$$CdCl^+(Asp)\ [282] + n\ hv \rightarrow CdCl^+(C_3H_5O_2N)\ [236] + H_2O + CO \quad (5)$$

$$CdCl^+(C_3H_5O_2N)\ [236] + n\ hv \rightarrow CdCl^+(C_2H_5N)\ [192] + CO_2 \quad (6)$$

These results differ from the previously studied $CdCl^+(Asn)$ and $CdCl^+(Gln)$ systems where only losses corresponding to NH_3 and CO were observed.[12,14] Here, replacement of the carboxamide group by the additional carboxylic acid group present in the Asp ligand allows for different reactions, dehydration rather than deamidation, to occur. Interestingly, $CdCl^+(Glu)$ also exhibited different fragmentation, with primary and secondary losses of H_2O and CO, respectively, but no subsequent CO_2 dissociation was observed.[15]

Nomenclature. Different conformations of intact complexes are named using nomenclature outlined previously.[12] In short, the complexes are designated by their metal binding site in brackets, with the deprotonation site (if present) indicated by a negative sign. In most systems, both the backbone and side chain carbonyls are binding sites with a subscript s (for side-chain) designating the latter. When binding takes place at the amino site, the nitrogen is always listed first, and the available oxygen binding sites are ranked such that the site with the shorter metal-binding site interaction is listed next. For several conformers, deprotonation does not occur at any of the metal binding sites. In these cases, the deprotonation site is given in curly brackets following the metal binding site. The designation of the metal binding site is also followed by the amino acid orientation, which is represented by the characterization of dihedral angles as cis (c,

for angles between 0° and 45°), gauche (g, 45° and 135°), or trans (t, 135° and 180°). In a few cases, signs of the gauche angles (+ or –) are also needed in order to distinguish otherwise identical names. Dihedral angles are measured starting from the backbone carboxylic acid hydrogen (unless this site is deprotonated) or the analogous proton on NH_2 in zwitterionic structures and going to the terminal side-chain carboxylic acid. When deprotonation occurs at a carbon along the backbone, standard nomenclature is used (α, β, γ …).

Zn(Asp-H)$^+$(ACN) Relative Energies. All levels of theory predict that the Zn(Asp-H)$^+$(ACN) ground structure (GS) (the lowest energy conformer) adopts a tetradentate [N,CO$^-$,CO$_s$](ACN) binding motif, where the metal binds to the backbone amino group, the carbonyl oxygen of the deprotonated backbone carboxylic acid group, the carbonyl oxygen of the side-chain carboxylic acid, and the nitrogen of the ACN group (see Table 1 and Figure 2). Two low-energy conformers of this type were found, where the [N,CO$^-$,CO$_s$]-ggtt(ACN) GS is located ~15 kJ/mol lower in energy than [N,CO$^-$,CO$_s$]-ggtc(ACN). Here, the ggtc carboxylic acid hydrogen has rotated so it no longer forms a hydrogen bond with the carbonyl (Figure 2), thus accounting for the increase in energy. Lying 22 – 23 and 43 – 44 kJ/mol higher in energy than the GS are [N,CO$_s^-$,CO](ACN) conformers with tggc and cggc geometries, respectively, in which deprotonation occurs at the side-chain carbonyl. Here, the preferential deprotonation of the backbone carboxylic acid is apparent, consistent with the related studies of Asn, Gln, and Glu.[12,14,15] Other higher energy tetradentate conformers given in Table 1 adopt [N$^-$,CO$_s$,CO](ACN), [N,CO$^-$,OH$_s$](ACN), [N,CO,CO$_s$]{C$_\beta^-$} (ACN), [CO$_2^-$,CO$_s$](ACN), [N,CO$_s^-$,OH](ACN), and [N,C$_\beta^-$,CO](ACN) binding motifs. An additional 21 higher energy species were also located and are given in the Supporting Information Table S1. Table S2 provides a full description of key geometric parameters of all conformers in Table 1. Notably, comparable Zn-ACN bond lengths are observed for all complexes (deviations within 0.02 Å). Select high-energy conformers are shown in Figure S6.

Comparison of Experimental and Theoretical IR Spectra: Zn(Asp-H)$^+$(ACN). In comparing the experimental and theoretical IR spectra below, it should be remembered that the

experimental IRMPD intensities are not always reproduced by the calculated one-photon linear absorption spectrum; however, IR spectra obtained using IRMPD methods are generally comparable to those recorded using linear absorption techniques, in part because the spectra result from incoherent, rather than coherent, multiple photon excitation. Previous modeling studies have demonstrated the near-linear absorption character of IRMPD studies.[37,40]

Figure 3 shows spectral comparisons of the $Zn(Asp\text{-}H)^+(ACN)$ experimental IRMPD action spectrum with IR spectra calculated for the five lowest-lying conformers, see Table 1. Here, major spectral features are located at 1749, 1656, 1577, 1438, 1398, 1247, 1182, 1142, and 1062 cm^{-1} in the experimental spectrum. Predicted bands of the $[N,CO^-,CO_s]$-ggtt(ACN) GS reproduce these experimental features well, especially in the high frequency region: 1750 cm^{-1}, uncoordinated backbone CO stretching and 1652 cm^{-1}, coordinated side-chain CO stretching. The band located at 1608 cm^{-1} in the calculated spectrum (NH_2 scissor) characteristically exhibits a red shift of about 25 cm^{-1} as a result of the strong anharmonic nature of this vibrational mode.[3,4,7,8,10,12] Accounting for the shift, this band can be assigned to the experimental band at 1577 cm^{-1}. At about 150 cm^{-1} lower, the calculated spectrum predicts a single, unresolved band centered between the two experimental bands at 1438 and 1398 cm^{-1}. The higher frequency 1438 cm^{-1} band is assigned to side-chain COH bending (where only the conformers characterized by a trans HOCC configuration exhibit a band in this region), although the predicted band is slightly red shifted compared to the experimental spectrum. The lower frequency band, assigned as side-chain CH_2 bending, exhibits a smaller shift blue shift. All lower frequency bands in the theoretical spectrum reproduce the experimental band frequencies well, although predicted intensities are systematically lower than experimental intensities. The spectral comparison for the low-lying $[N,CO^-,CO_s]$-ggtc(ACN) conformer is also given in Figure 3. This ggtc species exhibits a ~25 cm^{-1} blue shift of the coordinated side-chain CO stretch because this carboxylic acid is characterized by a cis HOCC configuration, thus changing the local CO environment. The poor agreement in the lower frequency region also suggests this conformer is not a major contributor to the measured spectrum. Similarly, predicted spectra for the next three higher energy conformers are shown,

where poor agreement in the diagnostic high frequency region suggest that these conformers are not significantly contributing to the experimental spectrum. Therefore, on a spectral basis, the [N,CO^-,CO_s]-ggtt(ACN) GS appears to be the primary populated species, consistent with a calculated equilibrium distribution of conformers at 298 K in which the [N,CO^-,CO_s]-ggtt(ACN) conformer has a population of ≥99.8%. Given in Supporting Information Table S3 are the scaled vibrational frequencies of the five lowest energy Zn(Asp-H)$^+$(ACN) conformers.

Comparison of Experimental and Theoretical IR Spectra: Zn(Asp-H)$^+$(Asp). Figure 4 shows structures of the lowest energy 6, 5, and 4-coordinate complexes of Zn(Asp-H)$^+$(Asp) located. In the 6 and 5-coordinate systems, the deprotonated Asp ligand adopts a tridentate [N,CO^-,CO_s] binding motif. Both the deprotonated and intact ligand adopt a bidentate conformation in the 4-coordinate system. Figure 4 shows both a yield and depletion spectrum, with the signal-to-noise ratio of the latter counterintuitively better than that of the yield spectrum. This suggests that many fragment ions were not detected because their intensities were below the noise level. The major spectral features of the experimental Zn(Asp-H)$^+$(Asp) spectrum are located at 1722 (with a shoulder around 1672), 1592 (observed in the depletion spectrum), 1411, 1150, and 1055 cm^{-1}, which are reproduced well by the GS hexadentate [N,CO^-,CO_s][N,CO_s,CO] conformer. In particular, bands at 1726 (primarily backbone uncoordinated CO stretching of the (Asp-H)$^-$ ligand), 1669 (side-chain CO stretching of both Asp ligands), 1403 (side-chain CH_2 bending of both ligands), 1158 (primarily COH bending of the neutral Asp ligand, with small contributions from side-chain COH bending of the (Asp-H)$^-$ ligand), and 1035 cm^{-1} (coordinated NH_2 wagging of both Asp ligands) reproduce the band frequencies and shapes well, with minor discrepancies in relative intensities of the lower frequency bands. Notably, the experimental band at 1592 cm^{-1} corresponds to the predicted bands at 1605 and 1627 cm^{-1}, which are characterized by NH_2 bending motions of the backbone amino group of the deprotonated and intact Asp ligands, respectively. As discussed above, this band is characteristically red shifted as a result of the strong anharmonic nature of the NH_2 bending vibrational mode. Accounting for this shift thereby explains the lower frequency of the experimental band.

Also given in Figure 4 are the calculated spectra for the pentadentate [N,CO^-,CO_s][N,CO] and tetradentate [N,CO^-][N,CO] Zn(Asp-H)$^+$(Asp) species. Both complexes exhibit more resolved bands in the high-frequency CO stretching region, not consistent with the one broad band in the experimental spectrum. Likewise, neither complex reproduces both 1150 and 1055 cm^{-1} bands in band position and intensity. For the tetradentate complex, which does reproduce the 1150 cm^{-1} band fairly well in intensity, no band is predicted at 1055 cm^{-1}, presumably because the bidentate conformation changes the local environment sufficiently that coordinated NH_2 wagging of both ligands is shifted. Overall, we conclude that the hexadentate GS isomer is the species formed experimentally.

Intact Zn(Asp-H)$^+$ versus Zn(Asp-H)$^+$(ACN) Relative Energies. In general, Zn(Asp-H)$^+$ complexes in which the deprotonated ligand remains intact have similar relative energetics compared to the Zn(Asp-H)$^+$(ACN) complexes with analogous binding motifs, compare Tables 1 and 2. Structures for Zn(Asp-H)$^+$ are directly analogous to those shown in Figure 2 after the ACN ligand is removed (see Figures S7 – S9). In particular, low-lying [N,CO^-,CO_s] and [N,CO_s^-,CO] species exhibit relative energies for both complexes with differences less than 4 kJ/mol. Overall, slightly longer metal-ligand bond interactions are observed in the Zn(Asp-H)$^+$(ACN) complexes because of the electron donation from the ACN to the metal center (Figure S9).

Comparison of Experimental and Theoretical IR Spectra: Intact Zn(Asp-H)$^+$. Interestingly, despite the structural and energetic similarities (see Supporting Information text and Figure S9) between the Zn(Asp-H)$^+$(ACN) (Figure 2 and Table 1) and Zn(Asp-H)$^+$ (Figure S7 and Table 2) complexes, very different spectral features are observed in their respective experimental spectra, Figure 1. In particular, there is no clear indication that the GS [N,CO^-,CO_s] tridentate species is formed experimentally for the Zn(Asp-H)$^+$ system because the measured spectrum shows very little intensity corresponding to uncoordinated CO stretching of the backbone carboxylate group, found at ~1750 cm^{-1} in the predicted spectra for [N,CO^-,CO_s] ggtt and ggtc low-energy conformers (Figures 5 and S10, respectively). Furthermore, none of the calculated

spectra reproduce the broadest band centered at 1444 cm^{-1}. The only predicted spectra that do not exhibit uncoordinated CO stretching of the backbone or side-chain carboxylate groups are the [N^-,CO,CO_s] and [N,CO,CO_s]{C_β^-} conformers, where deprotonation occurs at the nitrogen or backbone carbon, thus not allowing for a free CO stretch in the carboxylic acid groups. However, these conformers fail to reproduce the experimental bands at 1234 and 1294 cm^{-1}, as well as the intense, broad band centered at 1444 cm^{-1}, Figure 5. Furthermore, the relatively high energies of these systems suggests that the likelihood of these conformers strongly contributing to the spectrum is minimal. Nevertheless, an overview of additional higher energy $Zn(Asp\text{-}H)^+$ structures is given in Table S4. Table S5 provides structural information for all complexes in Table 2.

Given the definitive identification of the populated $Zn(Asp\text{-}H)^+(ACN)$ and $Zn(Asp\text{-}H)^+(Asp)$ complexes as having tridentate $(Asp\text{-}H)^-$ ligands, the lack of features consistent with a tridentate $Zn(Asp\text{-}H)^+$ complex in its experimental spectrum suggests that formation of $Zn(Asp\text{-}H)^+$ by irradiation of these complexes does not occur by simple ACN or Asp ligand loss. Rather, some other dissociation pathway is favored. Thus, additional structures that may be populated were explored computationally.

Rearranged $Zn(Asp\text{-}H)^+$ Relative Energies. Several lower energy complexes of a rearranged $(Asp\text{-}H)^-$ ligand are given in Table 3 and Figure 6. Which of these complexes might be formed experimentally cannot be accurately ascertained by a direct comparison of absolute energies. Thus, mechanistic pathways leading to these rearranged species were also located. For such rearranged $Zn(Asp\text{-}H)^+$ complexes, a similar nomenclature is used to identify the metal binding sites as outlined above, although here, the neutral formed from the rearrangement is identified as a ligand in parentheses. If hydrogen bonding (indicated by •) at this neutral is observed, this is indicated using a subscript, as detailed below. Deprotonated carbons retain the α, β, and γ label of the initial Asp species.

The lowest energy rearranged conformer located, $Zn(PA\text{-}H)^+[C_\alpha^-,CO_s](NH_{3,H\bullet OCO})$, adopts a binding motif where Asp has fragmented to form deprotonated propenoic acid (PA), NH_3, and CO_2, Figure 6. In this complex, the zinc metal center is bound to the deprotonated α carbon along

the backbone of PA, the carbonyl oxygen of PA, and the NH_3 group, with the CO_2 hydrogen bound to the ammonia. Alternatively, the CO_2 leaving group can remain bound via a weaker electrostatic interaction involving the Asp side-chain, $Zn(PA\text{-}H_{C\beta H\bullet OCO})^+[C_\alpha^-,CO_s](NH_3)$, which is associated with an energetic cost of ~13 kJ/mol, Table 3. The stability of these conformers is expected to be low because the loss of the weakly bound CO_2 ligand should occur facilely. Therefore, conformers characterized by an intact carboxylate backbone were also explored. The lowest energy conformer of this type that we located is characterized by a $Zn(Asp\text{-}NH_4)^+$ $[CO_2^-,CO_s](NH_3)$ binding motif, Figure 6, where zinc binds at the backbone carboxylate oxygens, the carbonyl oxygen of the side-chain carboxylic acid, along with the ammonia ligand. As shown in Table 3, we also explored the possibility of cyclization of these complexes, where the formation of a succinic anhydride (SA) structure is reasonable, especially given the observation that $C_4H_2O_3$ can be lost in reaction 2. Here, three conformers, $ZnOH^+(NH_3)(SA[CO])$, (Figure 6), $ZnOH^+(NH_{3,H\bullet OC})(SA[O])$ (Figure S11), and $ZnOH^+$(aSA[N,CO]) (Figure S11), were found where the latter involves the formation of an amino substituted succinic anhydride (aSA). These conformers are 56 – 70, 74 – 87 and 86 – 115 kJ/mol higher in energy than $Zn(PA\text{-}H)^+[C_\alpha^-,CO_s](NH_{3,H\bullet OCO})$, respectively. One conformer in Table 3 results from dehydration and decarboxylation of the complex such that H_2O remains bound to the zinc metal center. Such rearrangement leaves intact a ketone substituted ethanimine (3-oxo ethanimine), $Zn(OEA\text{-}H_{NH\bullet OCO})^+[N,C_\gamma^-](H_2O)$, where the CO_2 hydrogen bonds to the imine group, Figure S11. This complex is predicted to be 5 kJ/mol lower in energy than the $Zn(Asp\text{-}H)^+$ GS at the B3LYP level of theory and 19 – 40 kJ/mol higher in energy than the $Zn(Asp\text{-}H)^+$ GS at the remaining levels of theory. Select higher energy conformers of rearranged $Zn(Asp\text{-}H)^+$ are shown in Supporting Information Figure S11 and with energies in Table S6.

Comparison of Experimental and Theoretical IR Spectra: Rearranged $Zn(Asp\text{-}H)^+$. The calculated spectra for select rearranged $Zn(Asp\text{-}H)^+$ structures are given in Figure 5. The calculated spectrum for the lowest-energy structure, which formed the deprotonated PA ligand, (shown in green) reproduces several spectral features fairly well, although clearly does not reproduce the intense band peaking at ~1479 cm^{-1} nor does it account for the broad nature of the

1618 cm^{-1} experimental band. The alternate low-energy structure also containing the deprotonated PA ligand has a nearly identical spectrum, as shown in Figure S10. The only conformer predicted to reproduce the 1479 cm^{-1} band well is $Zn(Asp\text{-}NH_4)^+[CO_2^-,CO_s](NH_3)$ (shown in blue), where asymmetric CO_2 carboxylate stretching results in an intense band centered at 1483 cm^{-1}. At slightly lower frequencies (1434 and 1390 cm^{-1}), bands characterized by major motions of symmetric CO_2 stretching and COH bending, respectively, are also observed, thus corresponding to the experimental bands at 1444 and 1395 cm^{-1}. Furthermore, the highest frequency band, which peaks at 1618 cm^{-1} in the experimental spectrum but has a lower frequency shoulder, is explained nicely by motions at 1626 cm^{-1} (primarily C=C stretching with a minor contribution from C=O stretching) and 1598 cm^{-1} (primarily C=O stretching with minor contributions from C=C stretching). In addition, the experimental bands at 1160 (COH bending with additional contributions from CCH bending) and 1300 cm^{-1} (COH bending, CCH bending, and NH_3 umbrella motions) are reproduced reasonably well.

Calculated spectra for two additional conformers, $Zn(Asp\text{-}NH_4)^+[CO^-,CO_s](NH_3)$ and $ZnOH^+(NH_3)(SA[CO])$, are also given in Figure 5, where both conformers fail to reproduce the experimental spectrum. None of the located conformers reproduce the low-frequency band observed at 1234 cm^{-1}, a band that can be reproduced by the tridentate $Zn(Asp\text{-}H)^+[N,CO^-,CO_s]$ type structures, Figures 6 and S10. Likewise, this structure could account for a small peak at ~1730 cm^{-1}. The good agreement between the experimental and $Zn(Asp\text{-}NH_4)^+[CO_2^-,CO_s](NH_3)$ spectra suggests that this is the dominant complex contributing to the spectrum, although it does not reproduce the bands at 1234 and 1730 cm^{-1}. As detailed below, the dominance of this particular structure is consistent with reaction pathways leading to this low-energy rearranged species. The scaled vibrational frequencies of the five lowest energy intact and rearranged $Zn(Asp\text{-}H)^+$ conformers are given in Supporting Information Tables S7 and S8, respectively. Additionally, the spectral comparison between the experimental spectrum and calculated spectra for select higher energy intact and rearranged conformers is given in Figure S10.

Comparison of Experimental and Theoretical IR Spectra: $ZnOH^+(NH_3)(ACN)$. As discussed above, CO_2 laser irradiation of $Zn(Asp\text{-}H)^+(ACN)$ yields *m/z* 196 (where the IRMPD spectrum is assigned to $Zn(Asp\text{-}NH_4)^+(NH_3)$, Figure 5) and *m/z* 139 such that the IRMPD spectrum for this species was also measured, Figure S4. Here, IRMPD of *m/z* 139 induces losses of NH_3 and H_2O and both channels were included in the yield measurement. Two broad bands centered at 1272 and 675 cm^{-1} were observed, with no indication of a carbonyl group being present, given the absence of intense bands in the 1600 – 1800 cm^{-1} region. Thus, this species was identified as $ZnOH^+(NH_3)(ACN)$, whose calculated spectrum is also shown in Figure S4. The higher frequency 1272 cm^{-1} band corresponds well to the NH_3 umbrella motion predicted at 1277 cm^{-1}. The lower frequency band centered at 675 cm^{-1} is then characterized by the following motions: ZnOH bending (728 cm^{-1}, 70 km/mol); NH_2 wagging and ZnNH bending (662 cm^{-1}, 96 km/mol); ZnOH bending, NH_2 wagging, and ZnNH bending (639 cm^{-1}, 66 km/mol); and minor contributions of NH_2 twisting (636 cm^{-1}, 30 km/mol). (Here, each of the NH_2 motions identified here involve the two hydrogens furthest in proximity to the hydroxyl group.) Notably, the highest intensity predicted band at 662 cm^{-1} agrees nicely with the experimental observation, with contributions from the lesser intense bands determining the final position and intensity observed. An additional two bands of moderate intensity are predicted in the calculated spectrum at 1412 and 1628 cm^{-1}, but with much weaker intensities than the 1277 and 675 cm^{-1} bands. These lower intensities provide a likely reason for the failure to observe these two bands. Additionally, the band calculated at 1412 cm^{-1} involves CH_3 motions of the ACN ligand, in which case intramolecular vibrational redistribution (IVR)[41] may be inefficient, as postulated previously for an analogous ACN containing system.[42]

An isobaric $ZnNH_2^+(H_2O)(ACN)$ species was also located computationally and found to be about 60 kJ/mol higher in energy than $ZnOH^+(NH_3)(ACN)$. Its calculated spectrum (Figure S4) predicts two weak bands at 674 cm^{-1} (Zn-N stretching) and 750 cm^{-1} (NH_2 rocking), and one intense band at 1607 cm^{-1} (HOH bending). Although the predicted band at 674 cm^{-1} would correspond well to the experimental band at 675 cm^{-1}, the intensity of this band is predicted to be significantly lower than the other two bands. Furthermore, the absence of a band near 1607 cm^{-1}

(predicted to be the most intense) also suggests that this conformer is not populated, consistent with the high relative energy of this species. Thus, our energetic and spectral analyses indicate that the $ZnOH^+(NH_3)(ACN)$ species is populated, where no contributions from additional species are needed to reproduce the experimental spectrum. The identification of this conformer further affirms our conclusion that the precursor $Zn(Asp\text{-}H)^+$ ions readily undergo rearrangement processes.

$Zn(Asp\text{-}H)^+$ Rearrangement and Dissociation Pathways. The theoretical 0 K reaction coordinate for ACN dissociation from $Zn(Asp\text{-}H)^+(ACN)$ is characterized by a loose TS associated with a product asymptote of 209 – 222 kJ/mol, Figure 7 and Table 4. The relatively high energy here is interesting because in many systems, acetonitrile ligands can be thought of as weakly bound. Comparable energetics have been observed in previous metalated amino acid systems, e.g., the loss of ACN from $Zn(Ser\text{-}H)^+(ACN)$ requires slightly higher energies of 221 – 235 kJ/mol.[13] Despite this straightforward dissociation path, the spectroscopic evidence above clearly demonstrates that irradiation of $Zn(Asp\text{-}H)^+(ACN)$ with the CO_2 laser does not yield the intact $Zn(Asp\text{-}H)^+[N,CO^-,CO_s]$ complex, but rather the rearranged $Zn(Asp\text{-}NH_4)^+[CO_2^-,CO_s](NH_3)$ and $ZnOH^+(NH_3)(ACN)$ species. Thus, exploration of additional pathways for rearrangement of the $Zn(Asp\text{-}H)^+(ACN)$ complex characterized by similar energetic barriers is important. Here, we have located several pathways for rearrangement of $Zn(Asp\text{-}H)^+(ACN)$ and $Zn(Asp\text{-}H)^+$ leading to $Zn(Asp\text{-}NH_4)^+[CO_2^-,CO_s](NH_3)$, $Zn(PA\text{-}H)^+[C_\alpha^-,CO_s](NH_{3,H\bullet OCO})$, and $ZnOH^+(NH_3)(SA)$ complexes with and without the ACN ligand. Reaction coordinates are given in Supporting Information Figures S12 – S15, with relative energies given in Tables 4 and S9.

Two possibilities exist for the formation of $Zn(Asp\text{-}NH_4)^+[CO_2^-,CO_s](NH_3)$: rearrangement of $Zn(Asp\text{-}H)^+$ while the metal complex still interacts with ACN, or primary loss of ACN followed by the rearrangement. Both pathways parallel one another but the latter (which is detailed in Figure S12 and Table S9) requires about ~200 kJ/mol more energy than keeping the ACN ligand in the complex. The unfavorable energetics indicate that rearrangement of the

complex and formation of the NH_3 group must occur while maintaining binding to the ACN ligand. Notably, this is obviously the case for formation of the $ZnOH^+(NH_3)(ACN)$ product as well.

Key reaction species located for the pathway in which the ACN ligand remains are shown in Figure 7, and the full pathway (including all intermediate steps) is given in Figure S13, with relative energies for all reaction species given in Table 4. Here, $TS_{1R\text{-}ACN}$ (where "R" stands for *r*earrangement of the $Zn(Asp\text{-}H)^+[N,CO^-,CO_s]$-ggtt complex and ACN indicates the acetonitrile is present) is characterized by a ∠CCCC dihedral angle rotation. This motion forms $INT_{1R\text{-}ACN}$ in which both oxygens of the carboxylate are bound to Zn and the amino group has rotated away, making it more susceptible to accepting a proton. Such a proton transfer occurs from C_β in the following step, as the complex passes through rate-limiting $TS_{2R\text{-}ACN}$, 194 – 213 kJ/mol above the $Zn(Asp\text{-}H)^+(ACN)$ GS, Figure 7. Importantly, this TS is ~10 kJ/mol lower in energy than simple ACN loss, explaining why rearrangement can occur rather than dissociation of the ancillary ligand. This motion forms $INT_{2R\text{-}ACN}$, where the NH_3 group remains electrostatically bound to C_α. Elongation of this interaction occurs as the complex passes through $TS_{3R\text{-}ACN}$ and then $TS_{4R\text{-}ACN}$, resulting in the four-coordinate complex $INT_{4R\text{-}ACN}$, $Zn(Asp\text{-}NH_4)^+[CO^-,CO_s](NH_3)(ACN)$, 0 – 24 kJ/mol below $Zn(Asp\text{-}H)^+[N,CO^-,CO_s]$-ggtt(ACN), Figure 7.

From $INT_{4R\text{-}ACN}$, loss of ACN and NH_3 can occur facilely over loose transition states or rearrangements can occur that permit loss of CO_2 or SA. For CO_2 loss, the system passes over the tight rate-limiting $TS_{5RC\text{-}ACN}$, Figures S7 and S13, in which the C-CO_2 bond cleaves to form PA deprotonated at C_α. The incipient CO_2 ligand rotates away from Zn and remains hydrogen bound to the ammonia ligand in $INT_{5RC\text{-}ACN}$, $Zn(PA\text{-}H)^+[C_\alpha^-,CO_s](NH_{3,H\bullet OCO})(ACN)$. The CO_2 ligand is bound by only 109 – 132 kJ/mol, such that formation of the $Zn(PA\text{-}H)^+[C_\alpha^-,CO_s](NH_3)(ACN)$ + CO_2 products lies 113 – 127 kJ/mol below $TS_{5RC\text{-}ACN}$. For SA loss (where the detailed reaction coordinate is shown in Figure S14), the carboxylic acid group first rotates over TS_{5RSA} such that the hydroxyl group coordinates with Zn rather than the carbonyl group, forming INT_{5RSA}. Then the hydroxyl group migrates to the Zn facilitated by a backside attack at the carbon forming the succinic ring. This passes over TS_{6RSA} and forms the $ZnOH^+(NH_3)(ACN)(SA[O])$ complex, which

could lose any of the three ligands at sufficiently high energies. All levels of theory agree that SA is the most weakly bound of the three, and its loss yields the experimentally observed $ZnOH^+(NH_3)$(ACN) product. DFT levels of theory indicate that TS_{6RSA} is rate-limiting for SA loss and MP2 indicates the product asymptote is rate limiting. NH_3 and ACN dissociation are limited by loose TSs at all three levels of theory, where the product asymptotes for lie 9 – 47 and 14 – 52 kJ/mol, respectively, above the energies required for SA loss. We explored the possibility that a small amount of a $ZnOH^+(NH_3)$(SA[CO]) species (isobaric with $Zn(Asp\text{-}H)^+$) could be formed via ACN dissociation from $ZnOH^+(NH_3)$(ACN)(SA[O]). As shown in Figure 5, there is no evidence in the experimental spectrum for the intense band calculated at 1690 cm^{-1}, a coordinated CO stretch. Thus, our experimental results are consistent with dissociation of only SA from the $ZnOH^+(NH_3)$(ACN)(SA[O]) complex.

Overall, a comparison of the energetics for the various dissociation pathways of $Zn(Asp\text{-}H)^+[N,CO^-,CO_s]$(ACN) (loss of ACN, NH_3, CO_2, or SA) indicates that they are fairly similar, as shown in Figure 7. As noted above, irradiation of the $Zn(Asp\text{-}H)^+$(ACN) complex excites the molecule such that it rearranges over $TS_{2R\text{-}ACN}$, rather than lose the ACN ligand. Because the $INT_{4R\text{-}ACN}$ intermediate formed now has nearly 200 kJ/mol of energy, it will generally dissociate by the entropically most favorable reaction, as reflected by the 298 K Gibbs free energies, Table 4. In this case, loss of the ACN (reaction 1) or NH_3 ligands, which require no rearrangement can occur easily. (As shown in Figure S16, there is only a minor indication that this competitive loss of NH_3 is present at the strongest bands, consistent with the higher energy of this channel.) ACN loss from $INT_{4R\text{-}ACN}$ is favored by 24 – 25 kJ/mol over NH_3 loss across all levels of theory. These relative energetics and entropic effects explain why IR laser irradiation (either by FELIX or the CO_2 laser) of $Zn(Asp\text{-}H)^+[N,CO^-,CO_s]$-ggtt(ACN) leads to the dominant loss of SA in reaction 2 (the lowest energy process) but that rearrangement to $Zn(Asp\text{-}NH_4)^+(NH_3)$ species and loss of ACN in reaction 1 is competitive (lowest free energy process).

It can also be realized that once the rearranged $Zn(Asp\text{-}NH_4)^+(NH_3)$ species is formed, cooled radiatively, and then irradiated, it dissociates by loss of CO_2 in reaction 3 followed by loss

of NH_3 in reaction 4. This reaction coordinate is described in the Supporting Information text, shown in Figure S15 (energies in Table S9), and parallels that with the ACN ligand present, Figure 7. Reaction 3 dominates the dissociation now because formation of $Zn(PA\text{-}H)^+(NH_3)$ over TS_{5RC} (directly analogous to $TS_{5RC\text{-}ACN}$) is the lowest energy process available according to all three levels of theory, Table S9 and Figure S15, with sequential loss of the NH_3 ligand occurring easily with higher available energies.

Comparison of Experimental and Theoretical IR Spectra: $CdCl^+$(Asp). As shown in Figures 1 and 8, the major spectral features for the $CdCl^+$(Asp) complex are found at 1726 (with a shoulder at 1701), 1418, and 1162, with weak features at 1588 and 1057 cm^{-1}. These bands appear to be much more resolved than those observed in the $Zn(Asp\text{-}H)^+$ system, especially in the more diagnostic high-frequency range. These features are well reproduced by the predicted GS, [N,CO,CO_s]-tggtt, see Table 5 and Figure 9. (For a detailed description of higher energy conformers and key structural characteristics of these systems, see Supporting Information text, Figure S17, and Tables S10 and S11). Here, the calculated spectrum predicts two bands in the high frequency region at 1722 cm^{-1} (sym CO stretching) and 1686 cm^{-1} (asym CO stretching), which reproduce the experimental bands at 1726 and 1701 cm^{-1} well, although the two carbonyl bands are not resolved in the experimental spectrum. These results are similar to those reported for metalated Asp complexes of Li^+ and Cs^+, where the carbonyl bands (centered at ~1750 cm^{-1}) were not resolved, thus producing a single band in the carbonyl stretching region.[5] At about 100 cm^{-1} lower in frequency, the NH_2 bending motion is observed. As reported previously, this band characteristically exhibits a red shift of about 25 cm^{-1} as a result of the strong anharmonic nature of this vibrational mode.[3,4,7,8,10,12] A similar shift would produce a peak at 1591 cm^{-1}, in good agreement with the weak experimental band at 1588 cm^{-1}. Bands in the lower-frequency region (1418, 1162, and 1057 cm^{-1}) are also well reproduced by the calculated [N,CO,CO_s]-tggtt spectrum (1424 and 1418 cm^{-1}, unresolved motions of CH_2 bending and wagging as well as backbone and side-chain COH bending; 1168 and 1157 cm^{-1}, unresolved motions of amino NH_2 rocking as well as backbone and side-chain COH bending; and 1053 cm^{-1}, amino NH_2 wagging).

For the lowest energy zwitterionic conformers, [CO_2^-]-ctgtt and [CO_{2s}^-]-tggcc, the calculated spectra predict intense bands at about 1400 and 1450 cm^{-1} for which there is no evidence in the experimental spectrum. Interestingly, the calculated [N,CO]-tgttt spectrum predicts stretches corresponding to the main spectral features of the $CdCl^+$(Asp) spectrum, although there are significant intensity discrepancies observed for the two carbonyl stretches. Here, the bands at ~1730 cm^{-1} in the [N,CO,CO_s]-tggtt and [N,CO]-tgttt spectra are both characterized by symmetric CO stretching motions, although most of the motion corresponds to the side-chain CO stretch in the [N,CO]-tgttt system. Likewise, both systems predict a band at ~1700 cm^{-1}, asymmetric CO stretches, with most of the motion in the [N,CO]-tgttt system corresponding to the backbone CO, leading to an intensity equal to that of the higher frequency CO band. In addition, the COH bend of the side-chain shifts from 1418 cm^{-1} in the [N,CO,CO_s] structure to 1393 cm^{-1} for [N,CO], such that this experimental band is also more poorly reproduced by the latter structure.

On this basis, we conclude that the [N,CO,CO_s]-tggtt conformer is most likely to be the only conformer contributing significantly to the spectrum. Indeed, an equilibrium distribution of conformers at 298 K concluded that the predicted GS would have a population of ≥99.5% at all levels of theory. The scaled vibrational frequencies of the five lowest energy $CdCl^+$(Asp) conformers are given in Supporting Information Table S12.

Comparison to Zn^{2+} and Cd^{2+} Complexes with Asn. In many of our previous studies, Zn^{2+} and Cd^{2+} systems have been characterized by similar spectral features such that the main difference in the measured spectra and structural characteristics is a result of the identity of the metal involved in chelation (with additional effects resulting from the intact versus deprotonated nature of the amino acid ligand). In those cases, a comprehensive analysis of the spectral features exhibited in both experimental IRMPD action spectra elucidates important characteristics of the metal dependence of the two systems. However, a direct comparison of the experimental spectra found in the current study yields limited information regarding metal chelation effects, a result of the drastically different spectral features that appear to be more closely related to the nature of the

Asx ligands. Here, we find it useful to compare the results presented in this work to those previously reported for $Zn(Asn\text{-}H)^+$ and $CdCl^+(Asn)$.[14]

A comparative analysis of spectral features for the Asn and Asp complexes with Zn^{2+} and Cd^{2+} is shown in Figure S18. All complexes exhibit significantly different behavior in the high frequency region. For the cadmium complexes, the analysis is straightforward, where inherent differences of amide versus carboxylic acid interactions strongly affect this diagnostic region. For $CdCl^+(Asn)$, the amide and carboxylic acid groups of the Asn ligand reasonably produce two resolved carbonyl stretching bands at about 1645 and 1720 cm^{-1}. However, for $CdCl^+(Asp)$, both terminal groups are carboxylic acids such that these CO stretching motions are only differentiated by small local environment effects. Thus, the symmetric and asymmetric stretches are unresolved, producing one broad band in this region. More minor effects arise when considering additional motions, specifically amide NH_2 bending (at ~1590 cm^{-1} for $CdCl^+(Asn)$) and carboxylic acid COH bending (at ~1145 cm^{-1} in $CdCl^+(Asp)$ and $CdCl^+(Asn)$), as there are clearly no modes associated with amide NH_2 bending in the Asp complexes. Likewise, in the Asn complexes, only the backbone terminal group can be characterized by COH bending such that bands resulting from this motion are characteristically less intense in the $CdCl^+(Asn)$ spectrum.[14]

For the $Zn(Asn\text{-}H)^+$ and $Zn(Asp\text{-}H)^+$ systems, more distinct differences are observed primarily because the $(Asp\text{-}H)^-$ ligand has rearranged. Here, only the $Zn(Asn\text{-}H)^+$ spectrum exhibits a high frequency CO stretching band at ~1750 cm^{-1}, shown in Figure 10, characteristic of a single backbone CO stretch.[14] On this basis, the tridentate $Zn(Asn\text{-}H)^+[N,CO^-,CO_s]$-ggt GS conformer was identified as being present experimentally and could explain all bands except the band near 1500 cm^{-1} and the intensities of the bands at ~1300 and 1550 cm^{-1}. Because the $Zn(Asx\text{-}H)^+$ complexes are the first systems to exhibit rearrangement behavior, such a rearrangement was not considered previously because the dominant bands (in particular, the 1750 cm^{-1} backbone CO stretch) observed experimentally did correspond to the expected GS conformer.[14] However, if the analogous rearrangement (as observed in the Asp complexes, Figure 7) is considered, spectral evidence (bands between 1400 – 1500 cm^{-1} that correspond to asym and

sym carboxylate CO_2 stretching, and the band at ~1300, NH_3 umbrella) suggests that the $Zn(Asn\text{-}NH_4)^+[CO_2^-,CO_s](NH_3)$ complex was also formed experimentally, although to a smaller degree than observed in the Asp system. Comparison between the experimental spectrum and the calculated spectra for $Zn(Asn\text{-}H)^+[N,CO^-,CO_s]$-ggt and $Zn(Asn\text{-}NH_4)^+[CO_2^-,CO_s](NH_3)$ is shown in Figure 10. This comparison shows that the band at ~1500 cm^{-1} (indicative of carboxylate stretching in $Zn(Asn\text{-}NH_4)^+[CO_2^-,CO_s](NH_3)$) is observed with modest intensity (comparable to the 1750 cm^{-1} band) such that this complex appears to be an equal contributor to the spectrum. Indeed, a 60:40 (rearranged:intact) mixture of the two species was found to reproduce the experimental spectrum fairly well. This is consistent with reaction energetics that predict that simple ACN loss from $Zn(Asn\text{-}H)^+(ACN)$ (the precursor ion) is 10 – 24 kJ/mol *lower* in energy than the Asn ligand rearrangement pathway (that analogous to Figure 7), the opposite of the correlation observed in the current Asp analysis. Thus, the population of the intact $Zn(Asn\text{-}H)^+$ is expected to be greater than the analogous intact $Zn(Asp\text{-}H)^+$ species in the current study. Conversely, the spectral evidence for the $Zn(Asp\text{-}H)^+$ system suggests that the rearranged $Zn(Asp\text{-}NH_4)^+[CO_2^-,CO_s](NH_3)$ conformer is dominant, with only minor spectral indications that the tridentate $Zn(Asn\text{-}H)^+[N,CO^-,CO_s]$-ggtt GS is present.

Conclusions

IRMPD action spectra for complexes of aspartic acid cationized with Zn^{2+} and Cd^{2+} were measured in the region of 1000 – 1800 cm^{-1} and were compared to those calculated at the B3LYP/6-311+G(d,p) and B3LYP/def2-TZVP levels of theory, respectively. The theoretically determined GS for the $CdCl^+(Asp)$ complex is found to reproduce the experimental spectra well, as detailed in the discussion above. Here, tridentate $[N,CO,CO_s]$-tggtt is identified as the only complex being formed, where no additional contributions from higher energy conformers are needed to match the experimental spectrum. Likewise, the analogous $Zn(Asp\text{-}H)^+[N,CO^-,CO_s]$-ggtt(ACN) and $Zn(Asp\text{-}H)^+(Asp)$ $[N,CO^-,CO_s][N,CO_s,CO]$ complexes (predicted to be the GSs) match the experimental results for these two complexes well in all aspects. In contrast, the

analogous $Zn(Asp\text{-}H)^+[N,CO^-,CO_s]$-ggtt GS has a predicted spectrum with obvious differences from experimental results for $Zn(Asp\text{-}H)^+$ formed by CO_2 laser irradiation of the $Zn(Asp\text{-}H)^+(L)$ complexes where L = ACN or Asp. (A reviewer wonders whether the $Zn(Asp\text{-}H)^+$ complex could be generated in a vacuum system free of ACN. This seems possible although the competitive formation of $Zn(Asp\text{-}H)^+(Asp)$ in the present work demonstrates that ligation of this complex is strongly favored.) Instead, it is found that rearrangement occurs yielding the isobaric $Zn(Asp\text{-}NH_4)^+[CO_2^-,CO_s](NH_3)$ complex. The reaction pathway leading to this rearranged complex has a rate-limiting step that is lower in energy compared to simple ACN loss such that rearrangement dominates the dissociation of $Zn(Asp\text{-}H)^+(L)$ under CO_2 laser irradiation. Dissociation of the $Zn(Asp\text{-}H)^+(ACN)$ complex also forms $ZnOH^+(NH_3)(ACN)$, as confirmed by the comparison of its IRMPD spectrum to that of the calculated spectrum for the GS located theoretically. This identification confirms the facile rearrangement of the $(Asp\text{-}H)^-$ ligand, which can rearrange to form succinic anhydride along an extension of the path leading to $Zn(Asp\text{-}NH_4)^+(NH_3)$, Figure 7.

We also conclude that the analogous complex in the $Zn(Asn\text{-}H)^+$ system, $Zn(Asn\text{-}NH_4)^+[CO_2^-,CO_s](NH_3)$, was formed experimentally in a previous study,[14] although it exhibited a more minor contribution. On this basis, side-chain composition (carboxamide versus carboxylic acid) appears to have a significant effect on the stability of the deprotonated amino acid ligand. Overall, the analysis regarding the changes in vibrational modes and geometric parameters provides valuable information about binding of the metal center within the complex, a characterization instrumental in determining the metal dependence of these and other biologically relevant systems.

Acknowledgement. Financial support for this work was provided by the National Science Foundation, Grants CHE-1664618 and OISE-1357887. We gratefully acknowledge the *Nederlandse Organisatie voor Wetenschappelijk Onderzoek* (NWO) for the support of the FELIX

Laboratory. In addition, a grant of computer time from the Center of High Performance Computing at the University of Utah is greatly appreciated.

Supporting Information Available: Additional tables provide relative single point energies of high-energy $Zn(Asp-H)^+(ACN)$, intact $Zn(Asp-H)^+$, rearranged $Zn(Asp-H)^+$, and $CdCl^+(Asp)$ conformers; key geometric parameters of low-energy $Zn(Asp-H)^+(ACN)$, intact $Zn(Asp-H)^+$, and $CdCl^+(Asp)$ conformers; vibrational frequencies and IR intensities for the five lowest energy conformers of $Zn(Asp-H)^+(ACN)$, intact and rearranged $Zn(Asp-H)^+(ACN)$, and $CdCl^+(Asp)$ conformers; and relative single point energies for reaction species leading to the lowest energy rearranged species without the participation of ACN. Additional figures include representative mass spectra measured for the dissociation of $Zn(Asp-H)^+(L)$ (L = ACN and Asp), $Zn(Asp-H)^+$, and $CdCl^+(Asp)$ with and without FELIX; the IRMPD spectra of $Zn(Asp-H)^+$ formed from CO_2 irradiation of the $Zn(Asp-H)^+(ACN)$ precursor ion; spectral comparisons between the $ZnOH^+(NH_3)(ACN)$ IRMPD spectrum and its lowest energy conformer, the $Zn(Asp-H)^+$ IRMPD spectrum and low-energy intact $Zn(Asp-H)^+$ complexes as well as the lowest energy $ZnOH^+(NH_3)(SA[CO])$ species, and the IRMPD spectra of Zn^{2+} and Cd^{2+} complexes with Asn and Asp; structures of high-energy conformers of $Zn(Asp-H)^+(ACN)$, of intact and rearranged $Zn(Asp-H)^+$ complexes, and high-energy conformers of $CdCl^+(Asp)$ complexes; a structural comparison between intact $Zn(Asp-H)^+$ and $Zn(Asp-H)^+(ACN)$ complexes; and reaction coordinates mapping the formation of rearranged complexes (with and without the participation of ACN) as well as key dissociation pathways. This material is available free of charge via the Internet at http://pubs.acs.org.

References

(1) Oomens, J.; Moore, D. T.; Meijer, G.; von Helden, G., Infrared Multiple Photon Dynamics and Spectroscopy of Cationic PABA and Its Dehydroxylated Fragment Ion. *Phys. Chem. Chem. Phys.* **2004,** *6*, 710-718.

(2) Bush, M. F.; Forbes, M. W.; Jockusch, R. A.; Oomens, J.; Polfer, N. C.; Saykally, R. J.; Williams, E. R., Infrared Spectroscopy of Cationized Lysine and ε-N-Methyllysine in the Gas

Phase: Effects of Alkali-Metal Ion Size and Proton Affinity on Zwitterion Stability. *The Journal of Physical Chemistry A* **2007,** *111*, 7753-7760.

(3) Armentrout, P. B.; Rodgers, M. T.; Oomens, J.; Steill, J. D., Infrared Multiphoton Dissociation Spectroscopy of Cationized Serine: Effects of Alkali-Metal Cation Size on Gas-Phase Conformation. *J. Phys. Chem. A* **2008,** *112*, 2248-2257.

(4) Rodgers, M. T.; Armentrout, P. B.; Oomens, J.; Steill, J. D., Infrared Multiphoton Dissociation Spectroscopy of Cationized Threonine: Effects of Alkali-Metal Cation Size on Gas-Phase Conformation. *J. Phys. Chem. A* **2008,** *112*, 2258-2267.

(5) O'Brien, J. T.; Prell, J. S.; Steill, J. D.; Oomens, J.; Williams, E. R., Interactions of Mono- and Divalent Metal Ions with Aspartic and Glutamic Acid Investigated with IR Photodissociation Spectroscopy and Theory. *J. Phys. Chem. A* **2008,** *112*, 10823-10830.

(6) Heaton, A. L.; Bowman, V. N.; Oomens, J.; Steill, J. D.; Armentrout, P. B., Infrared Multiple Photon Dissociation Spectroscopy of Cationized Asparagine: Effects of Alkali-Metal Cation Size on Gas-Phase Conformation. *J. Phys. Chem. A* **2009,** *113*, 5519-5530.

(7) Citir, M.; Stennett, E. M. S.; Oomens, J.; Steill, J. D.; Rodgers, M. T.; Armentrout, P. B., Infrared Multiple Photon Dissociation Spectroscopy of Cationized Cysteine: Effects of Metal Cation Size on Gas-Phase Conformation. *Int. J. Mass Spectrom.* **2010,** *297*, 9-17.

(8) Carl, D. R.; Cooper, T. E.; Oomens, J.; Steill, J. D.; Armentrout, P. B., Infrared Multiple Photon Dissociation Spectroscopy of Cationized Methionine: Effects of Alkali-Metal Cation Size on Gas-Phase Conformation. *Phys. Chem. Chem. Phys.* **2010,** *12*, 3384-3398.

(9) Hofstetter, T. E.; Howder, C.; Berden, G.; Oomens, J.; Armentrout, P. B., Structural Elucidation of Biological and Toxicological Complexes: Investigation of Monomeric and Dimeric Complexes of Histidine with Multiply Charged Transition Metal (Zn and Cd) Cations Using IR Action Spectroscopy. *J. Phys. Chem. B* **2011,** *115*, 12648-12661.

(10) Citir, M.; Hinton, C. S.; Oomens, J.; Steill, J. D.; Armentrout, P. B., Infrared Multiple Photon Dissociation Spectroscopy of Cationized Histidine: Effects of Metal Cation Size on Gas-Phase Conformation. *J. Phys. Chem. A* **2012,** *116*, 1532-1541.

(11) Coates, R. A.; McNary, C. P.; Boles, G. C.; Berden, G.; Oomens, J.; Armentrout, P. B., Structural Characterization of Gas-Phase Cysteine and Cysteine Methyl Ester Complexes with Zinc and Cadmium Dications by Infrared Multiple Photon Dissociation Spectroscopy. *Phys. Chem. Chem. Phys.* **2015,** *17*, 25799-25808.

(12) Boles, G. C.; Coates, R. A.; Berden, G.; Oomens, J.; Armentrout, P. B., Experimental and Theoretical Investigations of Infrared Multiple Photon Dissociation Spectra of Glutamine Complexes with Zn^{2+} and Cd^{2+}. *J. Phys. Chem. B* **2015,** *119*, 11607-11617.

(13) Coates, R. A.; Boles, G. C.; McNary, C. P.; Berden, G.; Oomens, J.; Armentrout, P. B., Zn^{2+} and Cd^{2+} Cationized Serine Complexes: Infrared Multiple Photon Dissociation Spectroscopy and Density Functional Theory Investigations. *Phys. Chem. Chem. Phys.* **2016,** *18*, 22434-22445.

(14) Boles, G. C.; Coates, R. A.; Berden, G.; Oomens, J.; Armentrout, P. B., Experimental and Theoretical Investigations of Infrared Multiple Photon Dissociation Spectra of Asparagine Complexes with Zn^{2+} and Cd^{2+} and Their Deamidation Processes. *J. Phys. Chem. B* **2016,** *120*, 12486-12500.

(15) Boles, G. C.; Owen, C. J.; Berden, G.; Oomens, J.; Armentrout, P. B., Experimental and Theoretical Investigations of Infrared Multiple Photon Dissociation Spectra of Glutamic Acid Complexes with Zn^{2+} and Cd^{2+}. *Phys. Chem. Chem. Phys.* **2017,** *19,* 12394-12406.

(16) Iuchi, S., Three Classes of C_2H_2 Zinc Finger Proteins. *Cell. Mol. Life Sci.* **2000,** *58*, 625-635.

(17) Laity, J. H.; Lee, B. M.; Wright, P. E., Zinc Finger Proteins: New Insights into Structural and Functional Diversity. *Curr. Opin. Struct. Biol.* **2001,** *11*, 39-46.

(18) Rich, A. M.; Bombarda, E.; Schenk, A. D.; Lee, P. E.; Cox, E. H.; Spuches, A. M.; Hudson, L. D.; Kieffer, B.; Wilcox, D. E., Thermodynamics of Zn^{2+} Binding to Cys_2His_2 and $Cys_2HisCys$ Zinc Fingers and a Cys_4 Transcription Factor Site. *J. Am. Chem. Soc.* **2012,** *134*, 10405-10418.

(19) Malgierie, G.; Zaccaro, L.; Leone, M.; Bucci, E.; Esposito, S.; Baglivo, I.; del Gatto, A.; Russo, L.; Scandurra, R.; Pedone, P. V., et al., Zinc to Cadmium Replacement in the A. Thaliana Superman Cys_2His_2 Zinc Finger Induces Structural Rearrangements of Typical DNA Base Determinant Positions. *Biopolymers* **2011,** *95*, 801-810.

(20) Malgierie, G.; Palmieri, M.; Esposito, S.; Maione, V.; Russo, L.; Baglivo, I.; de Paola, I.; Milardi, D.; Diana, D.; Zaccaro, L., et al., Zinc to Cadmium Replacement in the Prokaryotic Zinc-Finger Domain. *Metallomics* **2014,** *6*, 96-104.

(21) Robinson, N. E.; Robinson, A. B., *Molecular Clocks: Deamidation of Asparaginyl and Glutaminyl Residues in Peptides and Proteins*. Althouse Press: Cave Junction, OR, 2004.

(22) Nilsson, M. R.; Driscoll, M.; Raleigh, D. P., Low Levels of Asparagine Deamidation Can Have a Dramatic Effect on Aggregation of Amyloidogenic Peptides: Implications for the Study of Amyloid Formation. *Protein Sci.* **2002,** *11*, 342-349.

(23) Oepts, D.; van der Meer, A. F. G.; van Amersfoort, P. W., The Free-Electron-Laser User Facility Felix. *Infrared Phys. Technol.* **1995,** *36*, 297-308.

(24) Valle, J. J.; Eyler, J. R.; Oomens, J.; Moore, D. T.; van der Meer, A. F. G.; von Heldon, G.; Meijer, G.; Hendrickson, C. L.; Marshall, A. G.; Blakney, G. T., Free Electron Laser-Fourier Transform Ion Cyclotron Resonance Mass Spectrometry Facility for Obtaining Infrared Multiphoton Dissociation Spectra of Gaseous Ions. *Rev. Sci. Instrum.* **2005,** *76*, 023103.

(25) Polfer, N. C.; Oomens, J.; Moore, D. T.; von Helden, G.; Meijer, G.; Dunbar, R. C., Infrared Spectroscopy of Phenylalanine Ag(I) and Zn(II) Complexes in the Gas Phase. *J. Am. Chem. Soc.* **2006,** *128*, 517-525.

(26) Polfer, N. C.; Oomens, J., Reaction Products in Mass Spectrometry Elucidated with Infrared Spectroscopy. *Phys. Chem. Chem. Phys.* **2007,** *9*, 3804-3817.

(27) Marshall, A. G.; Wang, T. C. L.; Ricca, T. L., Tailored Excitation for Fourier Transform Ion Cyclotron Resonance Mass Spectrometry. *J. Am. Chem. Soc.* **1985,** *107*, 7893-7897.

(28) Guan, S. H.; Marshall, A. G., Stored Waveform Inverse Fourier Transform (SWIFT) Ion Excitation in Trapped-Ion Mass Spectometry: Theory and Applications. *Int. J. Mass Spectrom. Ion Processes* **1996,** *158*, 5-37.

(29) Lemaire, J.; Boissel, P.; Heninger, M.; Mauclaire, G.; Bellec, G.; Hestdagh, H.; Simon, A.; Le Caer, S.; Ortega, J. M.; Glotin, F., et al., Gas Phase Infrared Spectroscopy of Selectively Prepared Ions. *Phys. Rev. Lett.* **2002,** *89*, 273002.

(30) Dunbar, R. C., Infrared Radiative Cooling of Isolated Polyatomic Molecules. *J. Chem. Phys.* **1989,** *90*, 7369-7375.

(31) Frisch, M. J.; Trucks, G. W.; Schlegel, H. B.; Scuseria, G. E.; Robb, M. A.; Cheeseman, J. R.; Scalmani, G.; Barone, V.; Mennucci, B.; Petersson, G. A., et al. *Gaussian 09*, Revision D.01; Gaussian, Inc.: Wallingford CT, 2009.

(32) Weigend, F.; Ahlrichs, R., Def2-SVP Basis Sets. *Phys. Chem. Chem. Phys.* **2005,** *7*, 3297-3305.

(33) Andrae, D.; Haeussermann, U.; Dolg, M.; Stoll, H.; Preuss, H., Energy-Adjusted Ab Initio Pseudopotentials for the Second and Third Row Transition Elements. *Theor. Chim. Acta* **1990,** *77*, 123-141.

(34) Feller, D., The Role of Databases in Support of Computational Chemistry Calculations. *J. Comput. Chem.* **1996,** *17*, 1571-1586.

(35) Grimme, S.; Ehrlich, S.; Goerigk, L., Effect of the Damping Function in Dispersion Corrected Density Functional Theory. *J. Comput. Chem.* **2011,** *32*, 1456-1465.

(36) Grimme, S.; Anthony, J.; Ehrlich, S.; Krieg, H., A Consistent and Accurate Ab Initio Parametrization of Density Functional Dispersion Correction (DFT-D) for the 94 Elements H-Pu. *J. Chem. Phys.* **2010,** *132*, 154104.

(37) Polfer, N. C., Infrared Multiple Photon Dissociation Spectroscopy of Trapped Ions. *Chem. Soc. Rev.* **2011,** *40*, 2211-2221.

(38) Kesharwani, M. K., Brauer, B., Martin, J. M. L. Frequency and Zero-Point Vibrational Energy Scale Factors for Double-Hybrid Density Functionals (and Other Selected Methods): Can Anharmonic Force Fields be Avoided? *J. Phys. Chem. A*. **2015,** *119,* 1701-1714.

(39) Berglund, M.; Wieser, M. E., Isotopic Compositions of the Elements 2009. *Pure Appl. Chem.* **2011,** *83*, 397-410.

(40) Oomens, J.; Sartakov, B. G.; Meijer, G.; von Helden, G., Gas-Phase Infrared Multiple Photon Dissociation Spectroscopy of Mass-Selected Molecular Ions. *Int. J. Mass Spectrom.* **2006,** *254*, 1-19.

(41) Shaffer, C. J.; Revesz, A.; Schröder, D.; Severa, L.; Teply, F.; Zins, E.-L.; Jasikova, L.; Roithova, J. Can Hindered Intramolecular Vibrational Energy Redistribution Lead to Non-Ergodic Behavior of Medium-Sized Ion Pairs? *Angew. Chem., Int. Ed*. **2012,** *51,* 10050−10053.

(42) Gao, J.; Bouwman, J.; Berden, G.; Oomens, J., The Influence of Metal Ion Binding on the IR Spectra of Nitrogen Containing PAHs. *J. Phys. Chem. A*. **2016,** *120,* 7800-7809.

Table 1. Relative Energies (0 K) and Gibbs Free Energies (298 K) of $Zn(Asp\text{-}H)^+(ACN)$ Complexes[a]

structure	B3LYP/**GD3BJ**[b]	B3P86	MP2(full)
$[N,CO^-,CO_s]$-ggtt(ACN)	0.0 (0.0) / **0.0 (0.0)**	0.0 (0.0)	0.0 (0.0)
$[N,CO^-,CO_s]$-ggtc(ACN)	15.2 (16.3) / **14.7 (15.8)**	14.9 (16.0)	14.8 (15.8)
$[N,CO_s^-,CO]$-tggc(ACN)	22.1 (23.2) / **21.8 (22.9)**	22.5 (23.6)	22.4 (23.5)
$[N,CO_s^-,CO]$-cggc(ACN)	43.1 (43.0) / **42.7 (42.6)**	43.2 (43.1)	43.8 (43.7)
$[N^-,CO_s,CO]$-tg_g+tt(ACN)	45.0 (47.1) / **47.7 (49.8)**	45.4 (47.5)	46.0 (48.1)
$[N,CO_s,CO]\{C_\beta^-\}$-tggtt(ACN)	47.1 (51.1) / **47.5 (51.5)**	43.7 (47.7)	52.5 (56.5)
$[N^-,CO_s,CO]$-tg+g_tt(ACN)	50.6 (52.0) / **53.3 (54.7)**	50.8 (52.2)	50.6 (52.1)
$[N,CO^-,OH_s]$-ggct(ACN)	53.9 (53.8) / **52.4 (52.3)**	57.1 (57.0)	49.2 (49.1)
$[N,CO_s,CO]\{C_\beta^-\}$-tggtc(ACN)	58.3 (62.6) / **58.6 (62.8)**	54.8 (59.0)	63.1 (67.3)
$[CO_2^-,CO_s]$-gcgt(ACN)	58.6 (58.0) / **66.2 (65.6)**	60.4 (59.9)	64.3 (63.7)
$[N^-,CO_s,CO]$-tggtc(ACN)	60.5 (63.0) / **63.2 (65.7)**	60.8 (63.3)	61.0 (63.5)
$[N^-,CO_s,CO]$-cggtt(ACN)	64.2 (64.9) / **66.7 (67.4)**	64.1 (64.8)	64.9 (65.6)
$[N,CO_s^-,OH]$-tggt(ACN)	66.0 (65.2) / **64.5 (63.6)**	69.4 (68.6)	62.4 (61.6)
$[N^-,CO_s,CO]$-tggtc(ACN)	66.4 (67.8) / **69.1 (70.5)**	66.5 (67.8)	66.1 (67.5)
$[CO_2^-,CO_s]$-gcgc(ACN)	72.1 (70.8) / **79.3 (78.0)**	73.7 (72.4)	77.3 (76.0)
$[N^-,CO_s,OH]$-tggtt(ACN)	82.0 (81.2) / **84.1 (83.3)**	85.5 (84.7)	81.7 (80.9)
$[N^-,CO_s,CO]$-cggtc(ACN)	82.1 (84.0) / **84.2 (86.1)**	81.9 (83.7)	82.5 (84.4)
$[N^-,CO_s]$-ttttt(ACN)	85.8 (82.1) / **94.0 (90.2)**	91.5 (87.8)	94.6 (90.8)
$[N,C_\beta^-,CO]$-tgttt(ACN)	89.1 (88.6) / **91.3 (90.8)**	85.5 (85.0)	85.3 (84.8)

[a] Relative single point energies at 0 K and 298 K free energies in parentheses calculated at the level of theory indicated using a 6-311+G(2d,2p) basis set. [b] Empirical dispersion corrected B3LYP-GD3BJ values are given in bold.

Table 2. Relative Energies (0 K) and Gibbs Free Energies (298 K) of Intact $Zn(Asp\text{-}H)^+$ Complexes[a]

structure	B3LYP/**GD3BJ**[b]	B3P86	MP2(full)
$[N,CO^-,CO_s]$-ggtt	0.0 (0.0) / **0.0 (0.0)**	0.0 (0.0)	0.0 (0.0)
$[N,CO^-,CO_s]$-ggtc	17.6 (17.7) / **18.8 (17.3)**	17.3 (17.3)	16.9 (16.9)
$[N,CO_s^-,CO]$-tggc	22.0 (20.7) / **23.8 (20.6)**	22.8 (21.5)	23.4 (22.1)
$[N^-,CO_s,CO]$-tg$_-$g$_+$tt	32.2 (32.0) / **36.5 (34.7)**	33.0 (32.8)	37.8 (37.6)
$[N,CO_s,CO]\{C_\beta^-\}$-tggtt	40.5 (41.8) / **40.9 (41.1)**	36.6 (37.9)	44.8 (46.2)
$[N^-,CO_s,CO]$-tg$_+$g$_-$tt	42.9 (42.4) / **47.3 (45.2)**	42.9 (42.3)	45.3 (44.8)
$[N,CO_s^-,CO]$-cggc	45.3 (43.8) / **46.6 (43.1)**	45.7 (44.2)	46.8 (45.3)
$[C_\beta H]\{C_\alpha^-\}$-tcttt	45.6 (28.1) / **61.2 (41.6)**	82.9 (65.4)	104.1 (86.6)
$[C_\beta H]\{C_\alpha^-\}$-ttttt	48.5 (30.9) / **63.0 (45.4)**	85.9 (68.2)	108.6 (91.0)
$[N^-,CO_s,CO]$-tggtc	50.3 (50.0) / **54.2 (52.4)**	50.8 (50.5)	55.1 (54.8)
$[N^-,CO_s,CO]$-cggtt	53.7 (53.5) / **57.5 (55.7)**	53.9 (53.7)	58.6 (58.3)
$[N,CO_s,CO]\{C_\beta^-\}$-tggtc	53.8 (55.1) / **55.9 (55.7)**	49.6 (50.9)	57.0 (58.2)
$[N^-,CO_s,CO]$-tggtc	61.2 (60.7) / **65.2 (63.1)**	60.9 (60.3)	63.0 (62.5)
$[N^-,CO_s,CO]$-cggtt	63.5 (63.0) / **67.4 (65.2)**	62.9 (62.3)	65.4 (64.8)
$[N,CO^-,OH_s]$-ggct	64.2 (62.7) / **64.0 (60.8)**	68.9 (67.4)	58.4 (56.8)
$[C_\beta H]\{C_\alpha^-\}$-tctct	69.4 (51.6) / **84.3 (64.6)**	107.9 (90.0)	128.6 (110.7)
$[OH_s]\{C_\alpha^-\}$-ttttc	70.3 (51.4) / **85.8 (72.9)**	107.2 (88.2)	129.2 (110.2)
$[C_\beta H]\{C_\alpha^-\}$-tttct	73.6 (55.1) / **88.3 (68.9)**	112.3 (93.9)	134.1 (115.7)
$[N,CO_s^-,OH]$-tggt	73.6 (71.2) / **73.5 (69.3)**	78.4 (75.9)	70.1 (67.7)
$[N^-,CO_s,CO]$-cggtc	74.0 (73.7) / **77.4 (75.6)**	73.9 (73.7)	78.3 (78.0)
$[C_\beta H]\{C_\alpha^-\}$-tcttc	74.6 (55.6) / **83.9 (71.0)**	111.6 (92.5)	132.9 (113.9)

[a] Relative single point energies at 0 K and 298 K free energies in parentheses calculated at the level of theory indicated using a 6-311+G(2d,2p) basis set. [b] Empirical dispersion corrected B3LYP-GD3BJ values are given in bold.

Table 3. Relative Energies (0 K) and Gibbs Free Energies (298 K) of Rearranged $Zn(Asp\text{-}H)^+$ Complexes[a]

structure	B3LYP/**GD3BJ**[b]	B3P86	MP2(full)
$Zn(PA\text{-}H)^+[C_\alpha^-,CO_s](NH_{3,H\bullet OCO})$	-131.3 (-158.3) / **-115.9 (-139.0)**	-94.0 (-121.0)	-103.2 (-130.3)
$Zn(PA\text{-}H_{C\beta H\bullet OCO})^+[C_\alpha^-,CO_s](NH_3)$	-118.6 (-150.3) / **-93.0 (-126.4)**	-81.2 (-112.9)	-90.2 (-122.0)
$Zn(Asp\text{-}NH_4)^+[CO_2^-,CO_s](NH_3)$	-89.3 (-101.2) / **-76.9 (-83.4)**	-73.2 (-85.0)	-70.5 (-82.3)
$Zn(Asp\text{-}NH_4)^+[CO^-,CO_s](NH_3)$	-83.2 (-96.7) / **-70.3 (-85.9)**	-60.0 (-73.5)	-48.2 (-61.7)
$Zn(PA\text{-}H)^+[C_\beta^-,CO_s](NH_{3,H\bullet OCO})$	-82.1 (-109.5) / **-66.2 (-88.5)**	-41.8 (-69.2)	-52.8 (-80.3)
$Zn(PA\text{-}H_{C\alpha H\bullet OCO})^+[C_\beta^-,CO_s](NH_3)$	-67.6 (-102.2) / **-39.0 (-68.8)**	-27.1 (-61.7)	-36.7 (-71.3)
$ZnOH^+(NH_3)(SA[CO])$	-66.7 (-84.3) / **-45.8 (-64.3)**	-38.1 (-55.7)	-43.6 (-61.2)
$ZnOH^+(NH_{3,H\bullet OC})(SA[O])$	-43.9 (-57.0) / **-30.3 (-45.1)**	-14.2 (-27.3)	-28.9 (-42.1)
$Zn(Asp\text{-}NH_3)^{2+}[CO,CO_s](NH_2^-)$	-28.4 (-40.1) / **-12.9 (-26.3)**	-1.2 (-12.9)	7.7 (-4.0)
$ZnOH^+$(aSA[N,CO])	-16.4 (-21.3) / **-5.5 (-11.9)**	-8.4 (-13.3)	-9.7 (-14.5)
$Zn(Ala\text{-}H)^+[N,C_\beta^-,CO](CO_2)$	-16.1 (-30.4) / **-3.0 (-18.5)**	2.6 (-11.8)	-14.6 (-29.0)
$Zn(\beta\text{-}Ala\text{-}H)^+[C_\alpha^-,CO](CO_2)$	-6.7 (-27.5) / **10.2 (-9.4)**	22.7 (2.0)	31.6 (10.8)
$Zn(OEA\text{-}H_{NH\bullet OCO})^+[N,C_\gamma^-](H_2O)$	-5.2 (-37.0) / **18.5 (-5.6)**	39.5 (7.7)	29.9 (-1.8)

[a] Single point energies relative to $Zn(Asp\text{-}H)^+[N,CO,CO_s]$ggtt at 0 K and 298 K free energies in parentheses calculated at the level of theory indicated using a 6-311+G(2d,2p) basis set. [b] Empirical dispersion corrected B3LYP-GD3BJ values are given in bold.

Table 4. Relative Energies (0 K) and Gibbs Free Energies (298 K) for Reaction Species Involved in the Rearrangement Pathways for $Zn(Asp\text{-}H)^+(ACN)$ [a]

structure	B3LYP	B3P86	MP2(full)
$Zn(Asp\text{-}H)^+[N,CO^-,CO_s]$-ggtt + ACN	208.5 (171.5)	214.6 (177.6)	222.4 (185.4)
$Zn(Asp\text{-}H)^+[N,CO^-,CO_s]$-ggtt(ACN)	0.0 (0.0)	0.0 (0.0)	0.0 (0.0)
$TS_{1R\text{-}ACN}$	97.0 (98.2)	105.4 (106.5)	114.3 (115.4)
$INT_{1R\text{-}ACN}$	58.7 (59.6)	60.5 (61.5)	64.3 (65.3)
$TS_{2R\text{-}ACN}$	201.6 (204.2)	193.7 (196.3)	212.8 (215.4)
$INT_{2R\text{-}ACN}$	121.5 (120.0)	121.0 (119.6)	128.8 (127.3)
$TS_{3R\text{-}ACN}$	129.4 (129.0)	138.1 (137.6)	156.6 (156.1)
$INT_{3R\text{-}ACN}$	98.9 (90.3)	120.5 (122.3)	117.5 (109.0)
$TS_{4R\text{-}ACN}$	99.4 (94.0)	122.3 (116.9)	119.7 (114.4)
$INT_{4R\text{-}ACN}$	-23.5 (-33.4)	-3.3 (-13.2)	0.1 (-9.9)
$TS_{5RC\text{-}ACN}$	110.8 (98.5)	132.4 (120.1)	127.1 (114.8)
$INT_{5RC\text{-}ACN}$	-125.2 (-152.8)	-97.1 (-124.7)	-117.4 (-145.1)
$Zn(PA\text{-}H)^+[C_\alpha^-,CO_s](NH_3)(ACN) + CO_2$	-16.4 (-68.6)	19.3 (-32.9)	14.1 (-38.1)
TS_{5RSA}	83.0 (76.9)	108.2 (102.1)	106.0 (99.9)
INT_{5RSA}	37.4 (33.4)	60.4 (56.4)	54.9 (50.9)
TS_{6RSA}	127.5 (122.3)	156.0 (150.9)	127.2 (122.1)
$ZnOH^+(NH_3)(ACN)(SA[O])$	41.4 (29.6)	70.2 (58.4)	48.8 (37.1)
$ZnOH^+(NH_3)(ACN) + SA$	104.8 (46.0)	136.0 (77.2)	143.5 (84.6)
$ZnOH^+(ACN)(SA[CO]) + NH_3$	136.9 (108.8)	173.1 (144.9)	174.4 (146.3)
$ZnOH^+(NH_3)(SA[CO]) + ACN$	141.7 (87.1)	176.5 (121.9)	178.8 (124.2)
$Zn(Asp\text{-}NH_4)^+[CO_2^-,CO_s](ACN) + NH_3$	114.6 (94.1)	138.5 (117.9)	147.7 (127.1)
$Zn(Asp\text{-}NH_4)^+[CO_2^-,CO_s](NH_3) + ACN$	119.2 (70.3)	141.4 (92.5)	152.0 (103.1)

[a] Relative single point energies and free energies in parentheses calculated at the level of theory indicated using a 6-311+G(2d,2p) basis set.

Table 5. Relative Energies (0 K) and Gibbs Free Energies (298 K) of $CdCl^+$(Asp) Complexes[a]

structure	B3LYP/**GD3BJ**[b]	B3P86	MP2(full)
[N,CO,CO_s]-tggtt	0.0 (0.0) / **0.0 (0.0)**	0.0 (0.0)	0.0 0.0
[CO_2^-]-ctgtt	18.3 (14.0) / **29.6 (25.6)**	20.1 (15.8)	29.3 (24.9)
[CO_{2s}^-]-tggcc	21.0 (17.1) / **32.2 (28.6)**	22.1 (18.2)	31.9 (28.0)
[N,CO_s,CO]-tggtc	24.8 (24.6) / **24.4 (24.3)**	24.7 (24.4)	24.9 (24.7)
[N,CO]-tgttt	26.4 (23.0) / **31.3 (28.6)**	27.2 (23.9)	33.9 (30.5)
[N,CO,CO_s]-cggtt	30.1 (29.8) / **29.8 (29.5)**	30.0 (29.7)	31.2 (30.8)
[N,CO_s,OH]-tggtt	30.4 (29.2) / **28.5 (27.7)**	32.0 (30.8)	27.6 (26.4)
[CO_{2s}^-]-ttgcc	31.6 (27.8) / **42.1 (38.1)**	34.0 (30.3)	41.3 (37.6)
[N,CO,OH_s]-tggct	38.4 (35.1) / **37.4 (35.3)**	40.5 (37.1)	36.1 (32.8)
[CO_2^-]-ctgtc	42.3 (38.1) / **53.0 (49.4)**	43.5 (39.3)	52.9 (48.7)
[CO_2^-]-ctggt	45.1 (38.6) / **55.9 (49.4)**	50.2 (43.7)	54.4 (47.9)
[N,CO]-tgtgt	47.6 (43.1) / **53.0 (48.3)**	50.7 (46.2)	54.9 (50.4)

[a] Relative single point energies at 0 K and 298 K free energies in parentheses calculated at the level of theory indicated using a def2-TZVPP basis set and SDD ECP for Cd. [b]Empirical dispersion corrected B3LYP-GD3BJ values are given in bold.

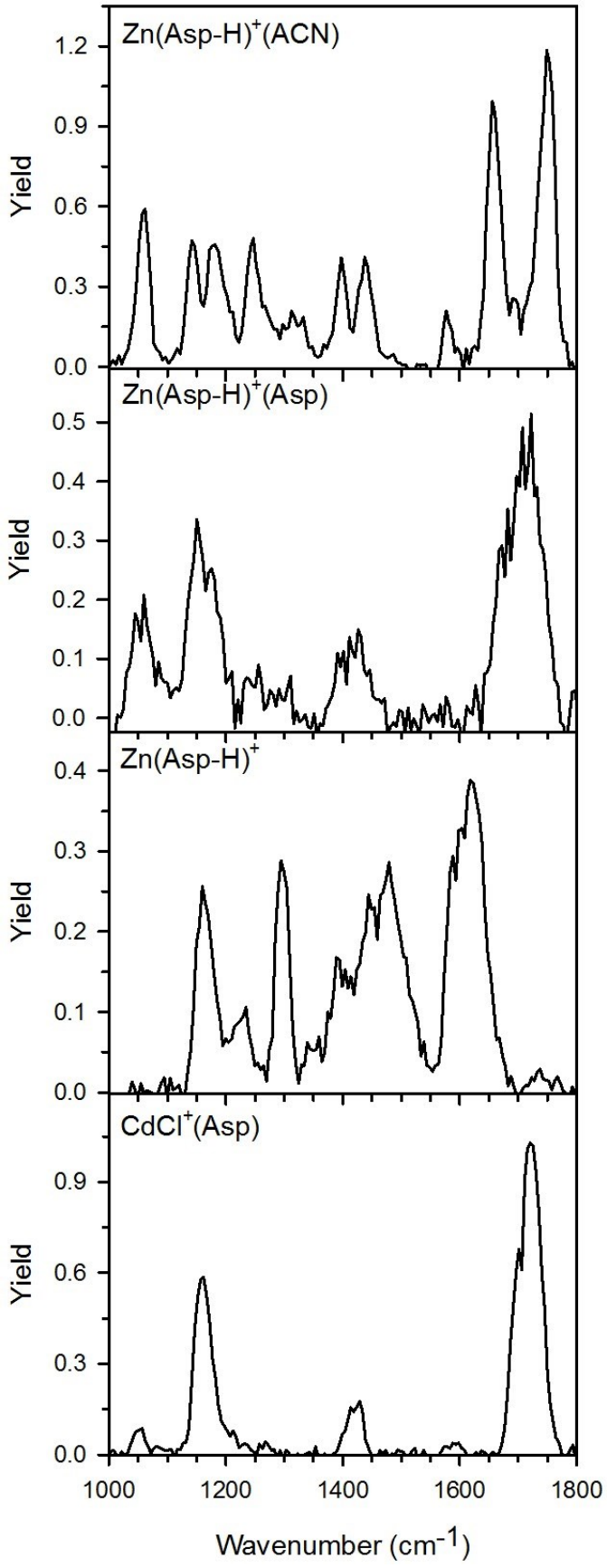

Figure 1. IRMPD action spectra of Zn^{2+} and Cd^{2+} complexes of Asp.

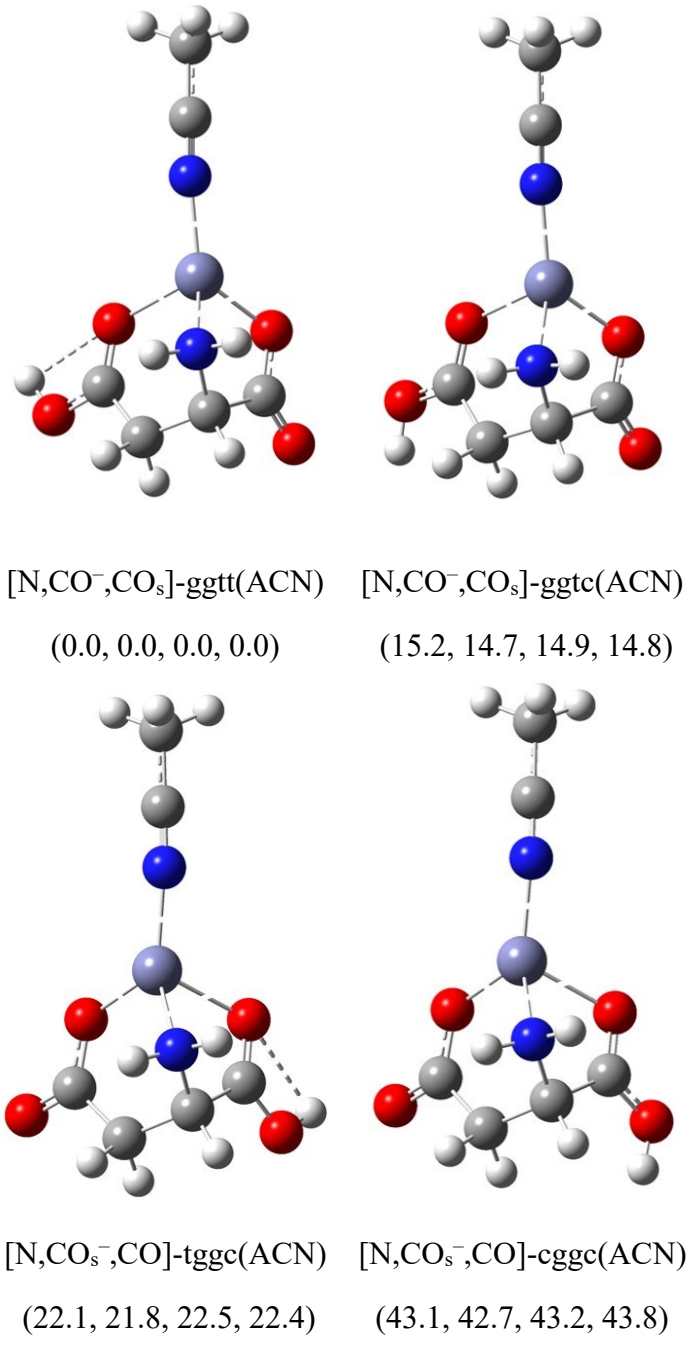

Figure 2. Structures of $Zn(Asp\text{-}H)^{+}(ACN)$ conformers calculated at the B3LYP/6-311+G(d,p) level of theory. Relative single point energies (0 K) are given at the B3LYP, B3LYP-GD3BJ, B3P86, and MP2(full) levels, respectively. Short dashed lines indicate hydrogen bonds. Metal-ligand interactions are shown by long dashed lines. (Red—oxygen, grey—carbon, white—hydrogen, blue—nitrogen, steel grey—zinc.)

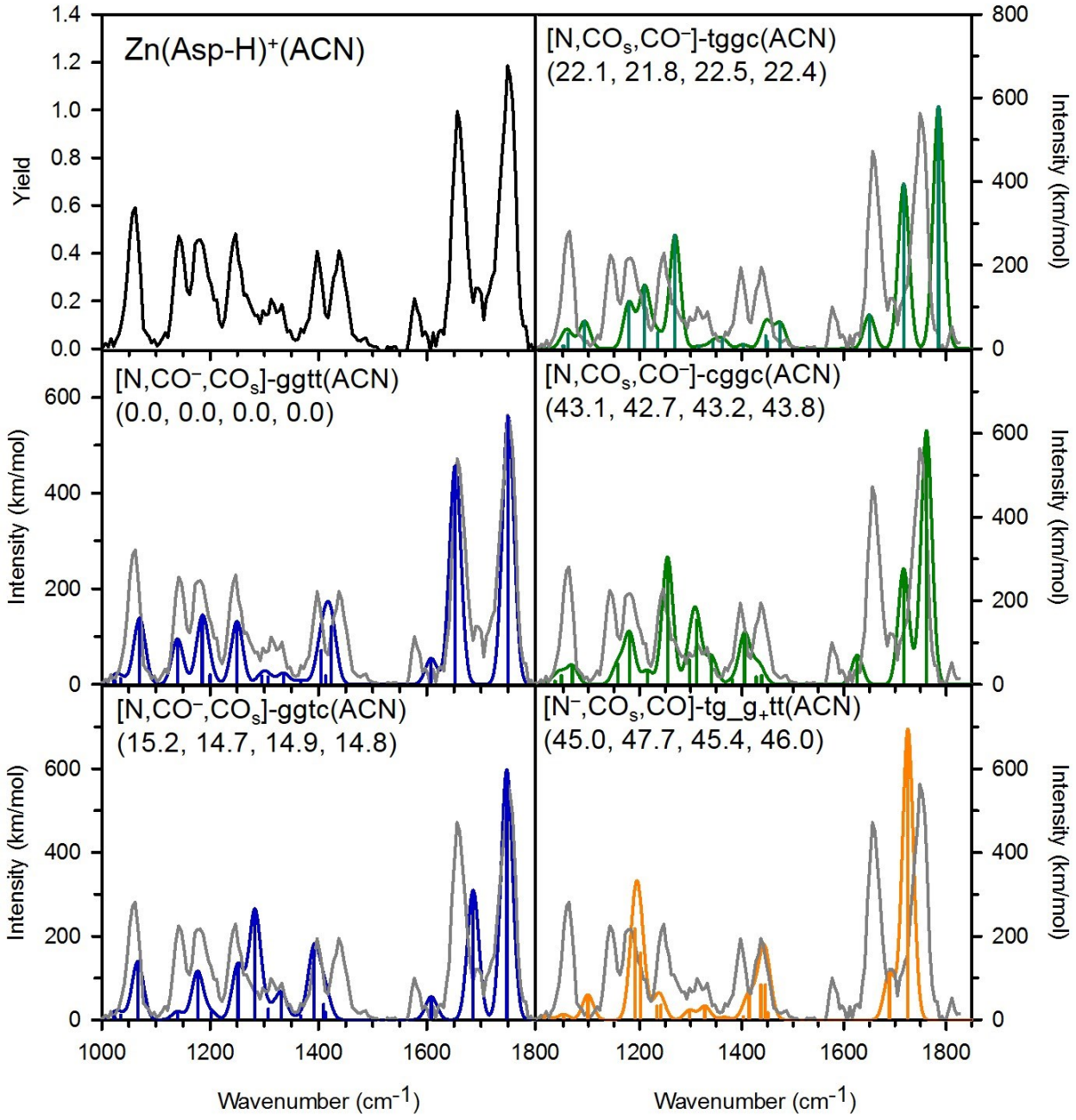

Figure 3. Comparison of the Zn(Asp-H)$^+$(ACN) experimental IRMPD action spectrum with IR spectra calculated at the B3LYP/6-311+G(d,p) level of theory for low-lying conformers. Relative 0 K energies (kJ/mol) are given at the B3LYP, B3LYP-GD3BJ, B3P86, and MP2(full) levels, respectively.

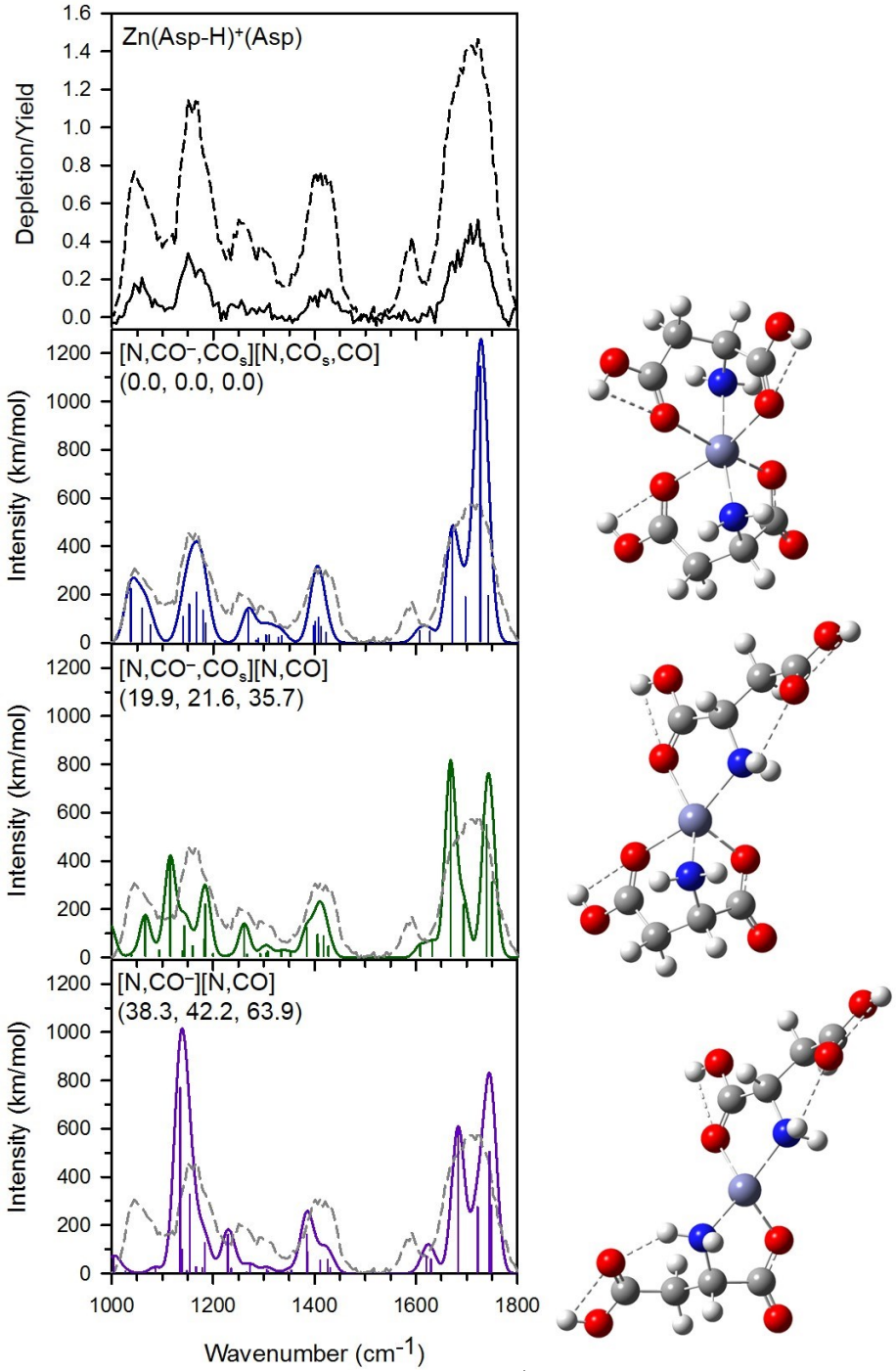

Figure 4. Comparison of the Zn(Asp-H)$^+$(Asp) experimental IRMPD action spectrum (shown as yield, solid black line, and depletion of the precursor ions, dashed black and grey lines) with IR spectra calculated at the B3LYP/6-311+G(d,p) level of theory for the lowest energy 6, 5, and 4-coordinate complexes located. In all structures, the deprotonated ligand is at the bottom. Relative 0 K energies (kJ/mol) are given at the B3LYP, B3P86, and MP2(full) levels, respectively. Short dashed lines indicate hydrogen bonds. Metal-ligand interactions are shown by long dashed lines. (Red—oxygen, grey—carbon, white—hydrogen, blue—nitrogen, steel grey—zinc.)

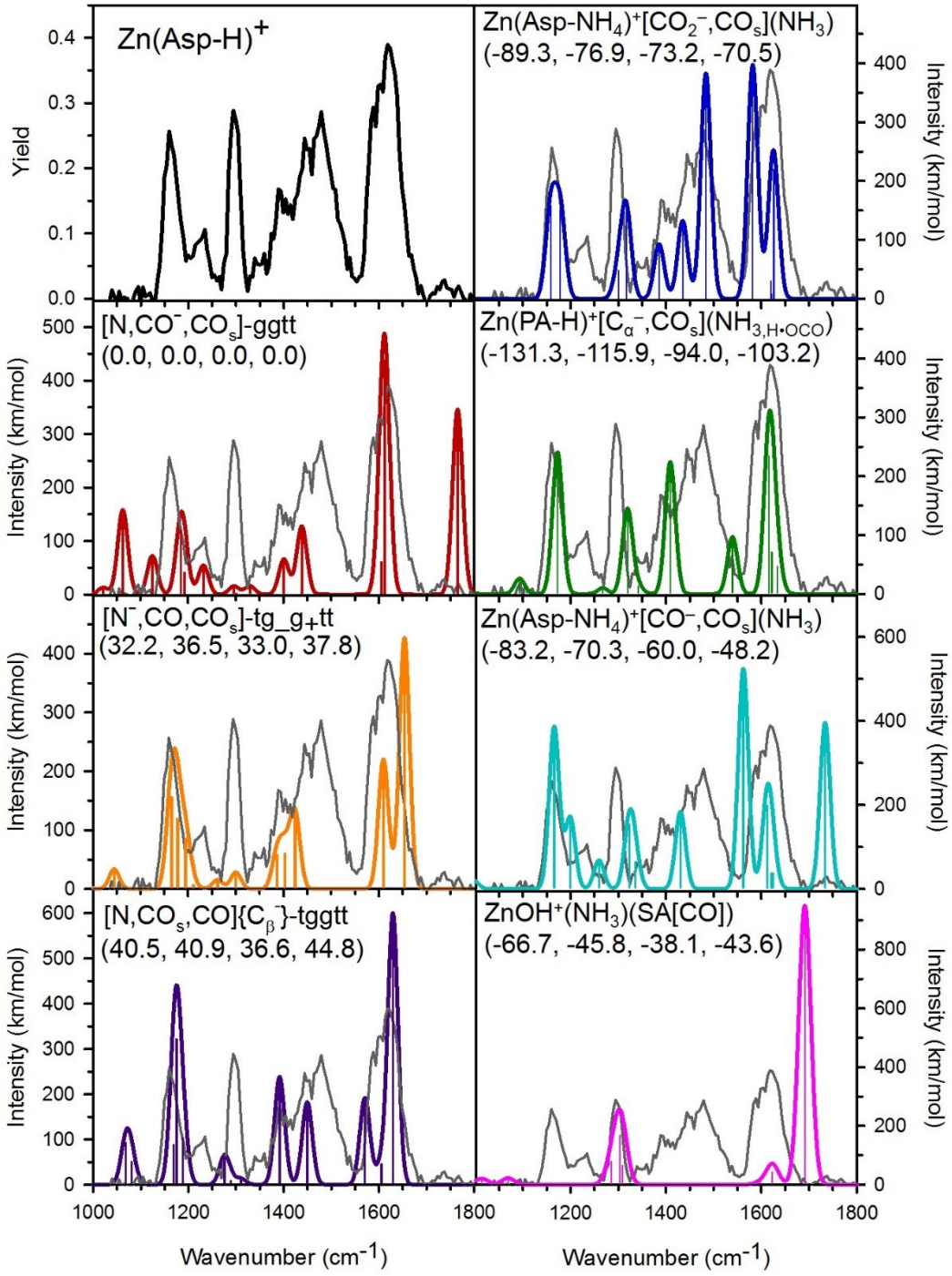

Figure 5. Comparison of the $Zn(Asp\text{-}H)^+$ experimental IRMPD action spectrum with IR spectra calculated at the B3LYP/6-311+G(d,p) level of theory for intact (left) and rearranged (right) $Zn(Asp\text{-}H)^+$ conformers. Relative 0 K energies (kJ/mol) are given at the B3LYP, B3LYP-GD3BJ, B3P86, and MP2(full) levels.

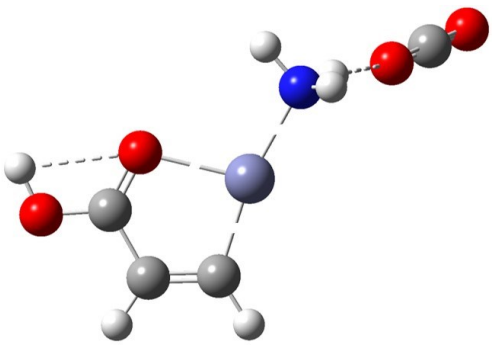

$Zn(PA\text{-}H)^+[C_\alpha^-,CO_s](NH_{3,H\bullet OCO})$

(-131.3, -115.9, -94.0, -103.2)

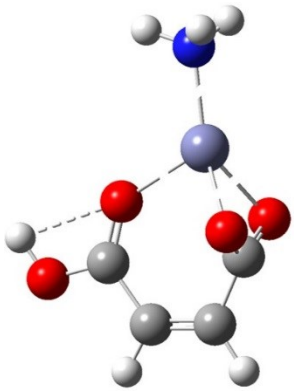

$Zn(Asp\text{-}NH_4)^+[CO_2^-,CO_s](NH_3)$

(-89.3, -76.9, -73.2, -70.5)

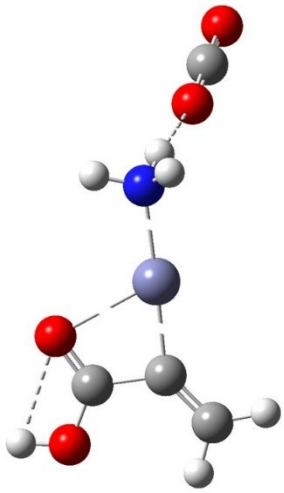

$Zn(PA\text{-}H)^+[C_\beta^-,CO_s](NH_{3,H\bullet OCO})$

(-82.1, -66.2, -41.8, -52.8)

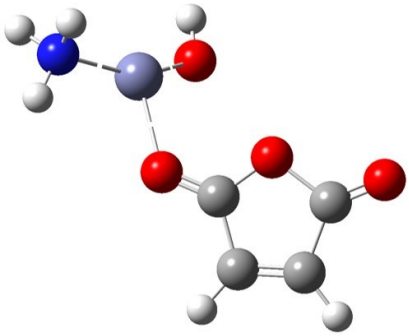

$ZnOH^+(NH_3)(SA[CO])$

(-66.7, -45.8, -38.1, -43.6)

Figure 6. Structures of select rearranged $Zn(Asp\text{-}H)^+$ conformers calculated at the B3LYP/6-311+G(d,p) level of theory. Single point energies (0 K) are given at the B3LYP, B3LYP-GD3BJ, B3P86, and MP2(full) levels, respectively, relative to $Zn(Asp\text{-}H)^+[N,CO^-,CO_s]$-ggtt. Short dashed lines indicate hydrogen bonds. Metal-ligand interactions are shown by long dashed lines. (Red—oxygen, grey—carbon, white—hydrogen, blue—nitrogen, steel grey—zinc.)

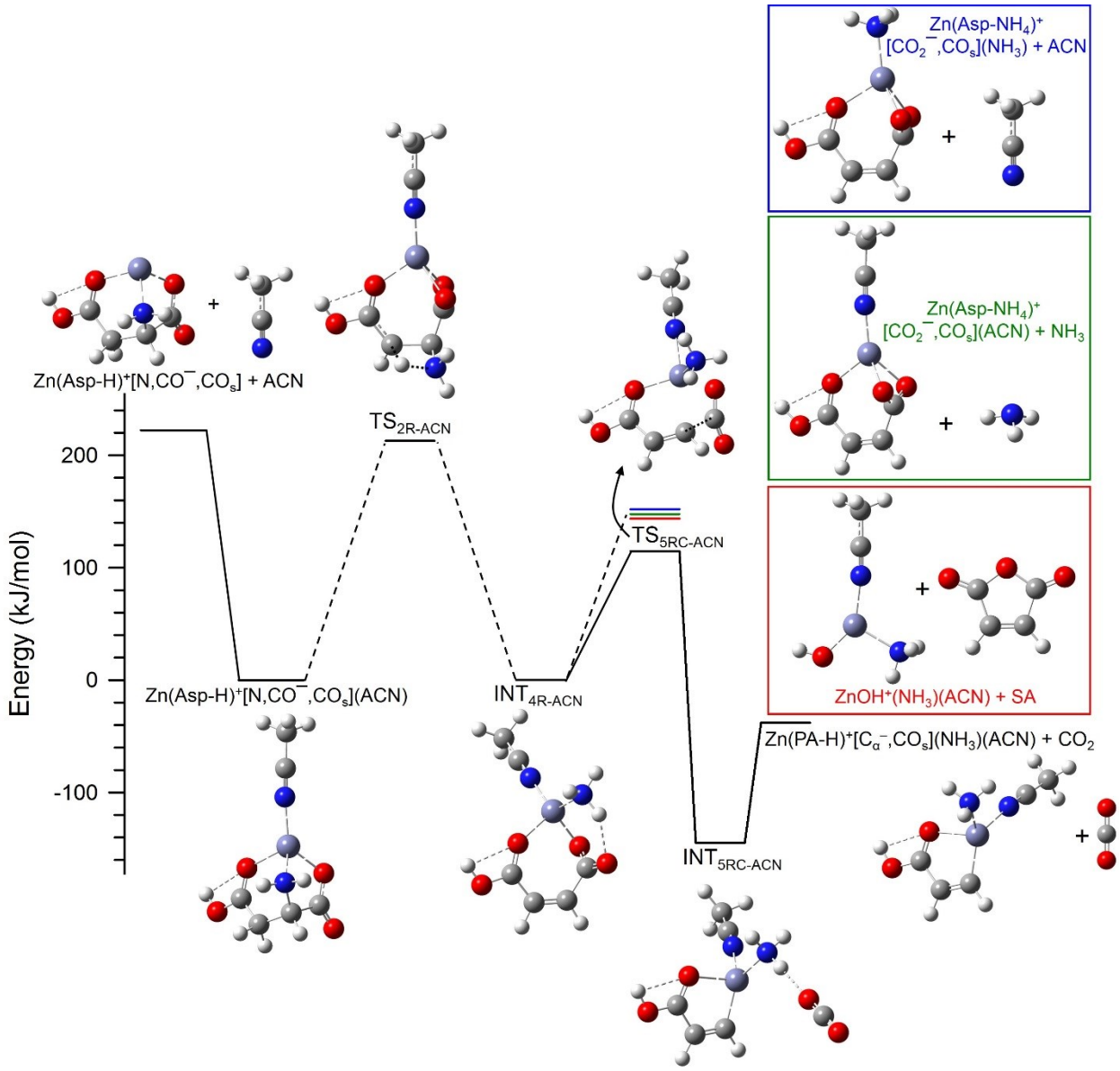

Figure 7. Major reaction species for dissociation of $Zn(Asp\text{-}H)^+[N,CO^-,CO_s](ACN)$ leading to $Zn(PA\text{-}H)^+[C_\alpha^-,CO_s](NH_3)(ACN)$ + CO_2, $ZnOH^+(NH_3)(ACN)$ + SA, $Zn(Asp\text{-}NH_4)^+[CO_2^-,CO_s](ACN)$ + NH_3, and $Zn(Asp\text{-}NH_4)^+[CO_2^-,CO_s](NH_3)$ + ACN. Structures calculated at the B3LYP/6-311+G(d,p) level of theory are shown along with single point energies calculated at the MP2(full)/6-311+G(2d,2p) level. Solid lines along the reaction coordinate indicate steps that are directly connected, and dashed lines indicate that intermediate steps were located (as shown in Figures S12 and S15). Short dashed lines indicate hydrogen bonds. Black dotted lines indicate bond cleavage or formation. Metal-ligand interactions are shown by long dashed lines. (Red—oxygen, grey—carbon, white—hydrogen, blue—nitrogen, steel grey—zinc.)

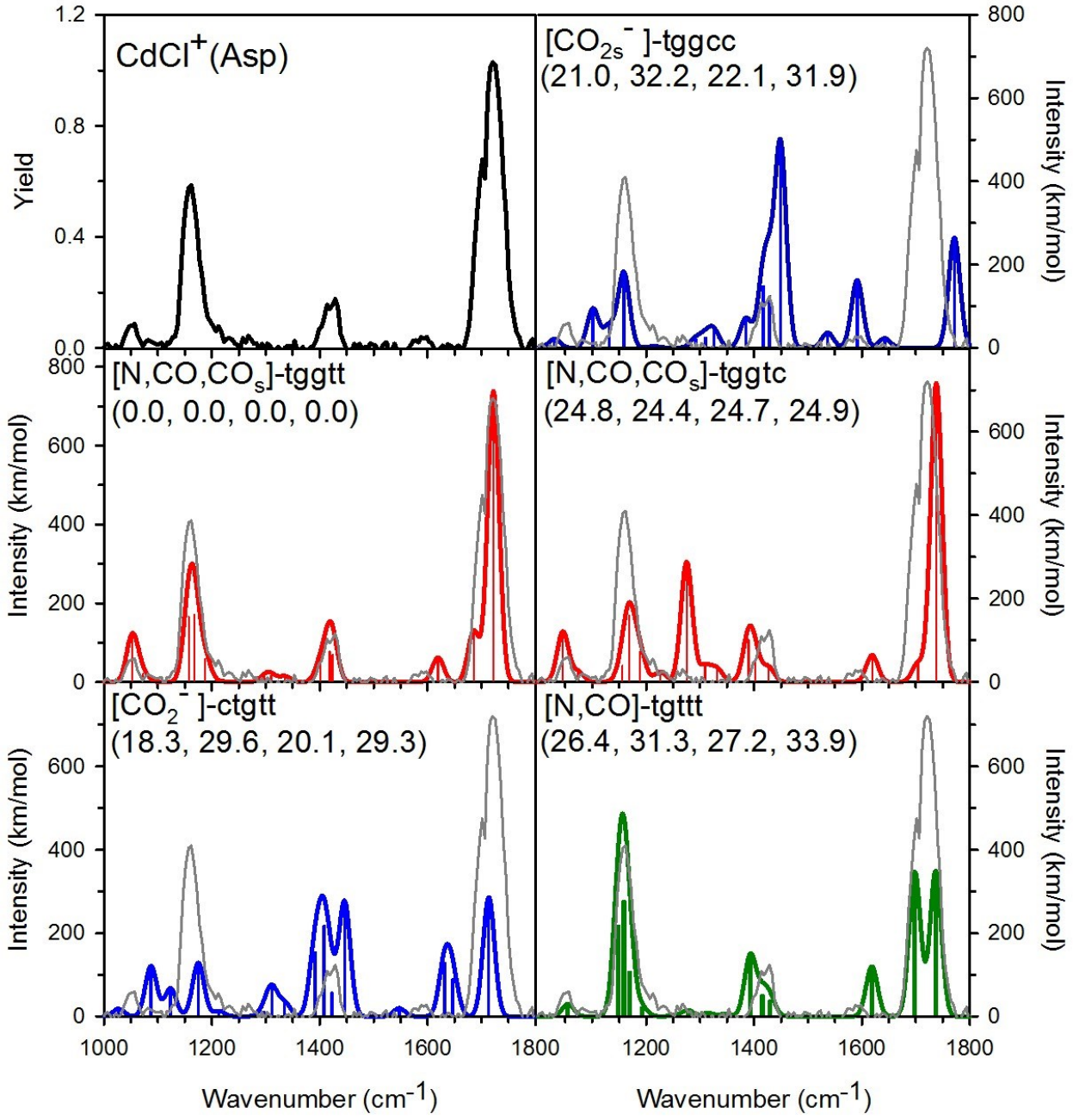

Figure 8. Comparison of the $CdCl^+$(Asp) experimental IRMPD action spectrum with IR spectra calculated at the B3LYP/def2-TZVP level of theory for low-lying conformers. Relative 0 K energies (kJ/mol) are given at the B3LYP, B3LYP-GD3BJ, B3P86, and MP2(full) levels, respectively.

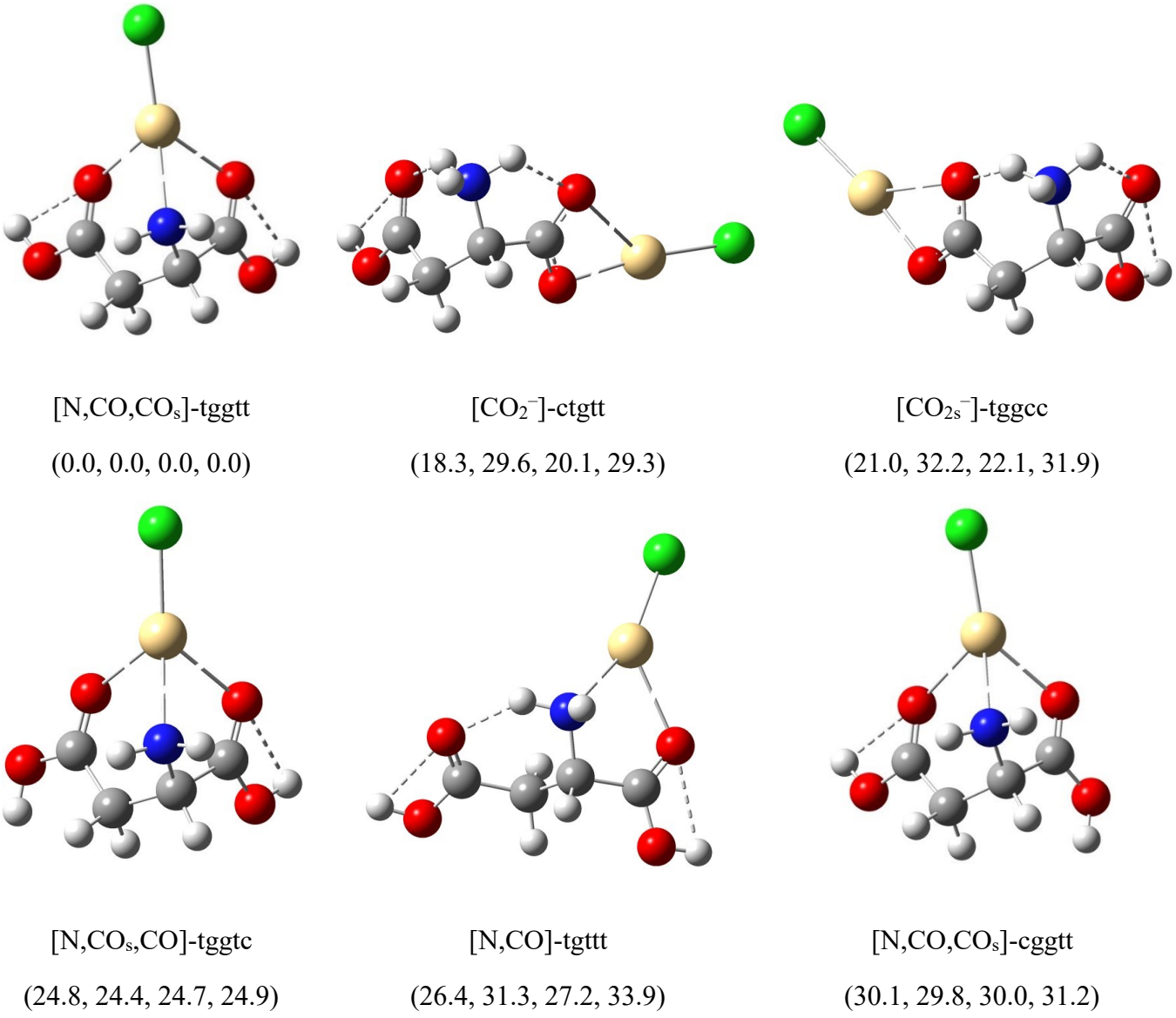

Figure 9. Structures of low-energy $CdCl^+$(Asp) conformers calculated at the B3LYP/def2-TZVP level of theory. Relative single point energies (0 K) are given at the B3LYP, B3LYP-GD3BJ, B3P86, and MP2(full) levels, respectively. Short dashed lines indicate hydrogen bonds. Metal-ligand interactions are shown by long dashed lines. (Red—oxygen, grey—carbon, white—hydrogen, blue—nitrogen, yellow—cadmium, green—chlorine.)

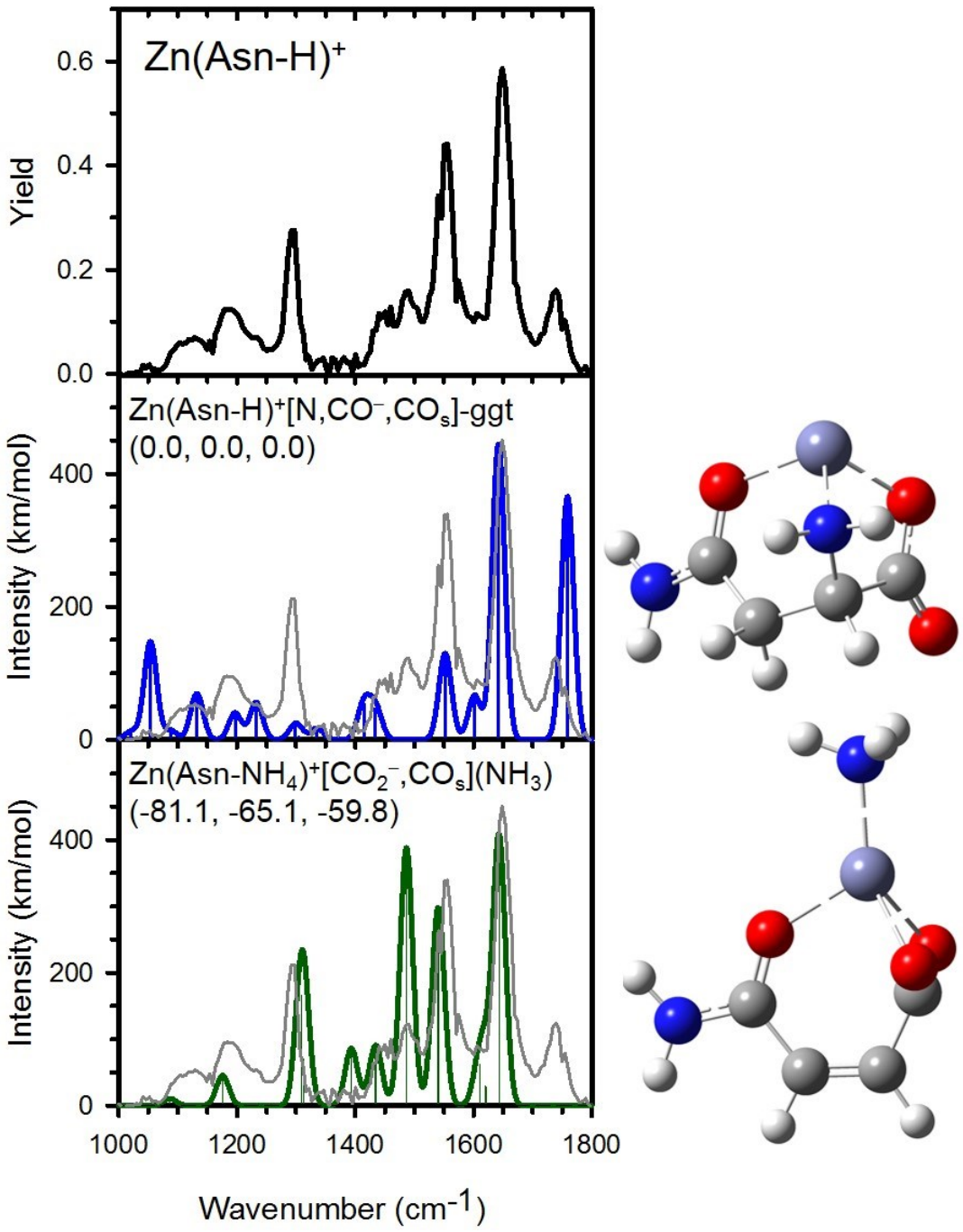

Figure 10. Comparison of the measured infrared multiple photon dissociation (IRMPD) action spectrum of $Zn(Asn\text{-}H)^+$ with spectra calculated at the B3LYP/6-311+G(d,p) level of theory for the observed tridentate and rearranged species.[14] Relative 0 K single point energies given at the B3LYP, B3P86, and MP2/6-311+G(2d,2p)//B3LYP/6-311+G(d,p) levels of theory, respectively. Metal-ligand interactions are shown by long dashed lines. (Red—oxygen, grey—carbon, white—hydrogen, blue—nitrogen, steel grey—zinc.)

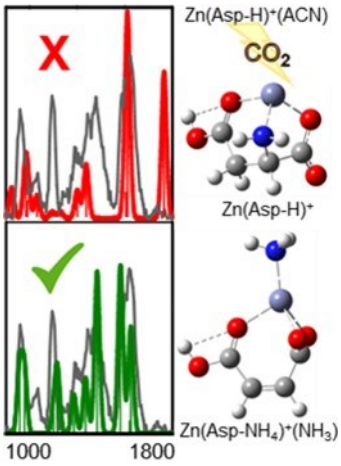

TOC Graphic